DL 98-007

A STUDY OF CONCENTRATION FLUCTUATIONS IN INSTANTANEOUS CLOUDS DISPERSING IN THE ATMOSPHERIC SURFACE LAYER FOR RELATIVE TURBULENT DIFFUSION: BASIC DESCRIPTIVE STATISTICS

EUGENE YEE
Defence Research Establishment Suffield, Box 4000, Medicine Hat, Alberta, T1A 8K6 Canada

P. R. KOSTENIUK
Kosteniuk Consulting Ltd, [illegible] 6th Street East Saskatoon, Saskatchewan, S7H 1B7 Canada

J. F. BOWERS
Meteorology Division, West Desert Test Center U.S. Army Dugway Proving Ground, Dugway, UT 84022–5000, USA

(Received in final form 4 March 1998)

Abstract. A series of tracer experiments studying the statistical properties of concentration fluctuations in clouds dispersing in the atmospheric surface layer is described and analyzed. Experiments were conducted at downwind fetches between about 200 and 1200 m, under a wide range of atmospheric conditions ranging from very unstable to moderately stable stratification. The present experiments have addressed basic requirements not met by past field experiments involving instantaneously released clouds; namely, the experiments provided repeat realizations of instantaneously released clouds measured with high-resolution concentration detectors, accompanied by the contemporaneous acquisition of high-quality meteorological and turbulence measurements.

Extensive analyses are performed on the cloud concentration data in the framework of relative diffusion. Ensembles of cloud concentration realizations have been constructed. From these ensembles, crosswind and time profiles of the ensemble-mean concentration, concentration variance, ensemble-mean dosage, and dosage variance are obtained. The behaviour of the time profiles of the integral time scale of cloud concentration fluctuations is studied. The use of surface-layer similarity theory for the analysis of the downwind variation of a number of cloud quantities (e.g., cloud size and duration, cloud centre ensemble-mean concentration and dosage, cloud centre concentration and dosage variance, cloud centre integral time scale) is shown to be an effective basis for ordering these quantities. Furthermore, a number of approximate universal relationships describing the behavior of these cloud quantities has been derived. Finally, it is shown that the scaled crosswind and time profiles of ensemble-mean concentration and concentration variance as well as the scaled time profiles of the concentration fluctuation integral time scale exhibit self-similar forms that are independent of atmospheric stratification and downwind fetch.

Key words: Cloud dispersion, Concentration fluctuations, Relative diffusion

1. Introduction

In recent years, it has been recognized that progress towards understanding turbulent diffusion in the atmosphere requires the characterization not only of mean

Boundary-Layer Meteorology **87**: 409–457, 1998.
© 1998 *Kluwer Academic Publishers. Printed in the Netherlands.*

concentrations, but also of statistics of concentration fluctuations. The random nature of turbulent motions of a large number of different scales in the atmosphere produces fluctuations of the instantaneous concentration in dispersing plumes or clouds. In consequence, field experiments studying concentration fluctuations in plumes released from continuously emitting sources have been conducted during the last few years (e.g., Hanna, 1984; Sawford et al., 1985; Dinar et al., 1988; Petersen et al., 1990; Mylne and Mason, 1991; Mylne, 1993; Yee et al., 1994a; Yee et al., 1995; among others). These studies have led to a substantial advance in our current understanding of the probabilistic and statistical characteristics of plumes dispersing in the turbulent motions of atmospheric boundary-layer flow.

Although there are now excellent datasets taken with fast-response concentration detectors documenting the nature of concentration fluctuations in plumes, there is still a need for similar measurements to be made in instantaneous clouds dispersing in the atmosphere. The sudden release of a quantity of contaminant into the atmosphere (e.g., from bombs, artillery shells, tank ruptures), and the subsequent dispersion of the instantaneous cloud formed from the release, is an important problem in both civilian and military risk analysis. Unfortunately, there has been relatively little effort expended in the measurement and investigation of concentration fluctuations in dispersing clouds resulting from instantaneous releases of a tracer into the atmosphere. A major difficulty is that an evolving cloud is an intrinsically nonstationary and inhomogeneous phenomenon, requiring the measurement of a large number of realizations (replications) of the dispersing cloud under the constraint that the conditions at release and in the atmosphere (e.g., mean wind and turbulence characteristics) are the same in each realization of the ensemble. In particular, achieving stationarity in atmospheric conditions over an extended measurement period is problematic, given the fact that atmospheric flows are generally time-dependent and inhomogeneous.

Experimental investigations devoted to the study of concentration fluctuations in instantaneous clouds are very limited so far. Meroney and Lohmeyer (1984) studied concentration fluctuations resulting from the sudden release of a volume of dense gas in a neutrally stable wind tunnel boundary layer. Zimmerman and Chatwin (1995) and Sweatman and Chatwin (1996) described statistical properties of instantaneous releases of dense gas measured in a wind tunnel by Hall et al. (1991). Yee et al. (1994b) investigated the statistical properties of the turbulent concentration field in a cloud dispersing in a near-neutral or slightly unstable surface layer using L-moments constructed from linear combinations of order statistics. These tracer experiments were limited to measurements of concentration fluctuations at fixed points downwind of a quasi-instantaneous release of a tracer for ranges between about 25 and 300 m. Furthermore, the small number of detectors available for these tracer experiments did not allow the cross-puff concentration structure to be investigated.

Because data from controlled field experiments will be needed for the validation of model and laboratory studies of concentration fluctuations in dispersing clouds,

and because full-scale atmospheric studies of the detailed structure of fluctuating cloud concentrations are virtually non-existent, we have designed and conducted a series of tracer experiments with the goal of providing more extensive measurements of concentration fluctuation statistics in a dispersing cloud. The general aim of this paper is to present some interesting measurements of the mean and fluctuating concentration and dosage in a dispersing cloud for relative diffusion. From the analysis of these measurements, a number of general features in the statistical description of the concentration fluctuations in a dispersing cloud can be discerned. In the present study, an attempt is made to provide a simple characterization of the cloud concentration and dosage statistics which retains salient and essential features in the cloud description. This is achieved using similarity hypotheses to provide a general framework for the data analysis that can be used to describe the cloud concentration statistics in terms of a few basic parameters.

2. Site, Instrumentation, and Experimental Procedures

The measurements were carried out in September 1996 at the Salt Flats Causeway Site on U.S. Army Dugway Proving Ground in northwestern Utah, 40°08′22″ N and 113°26′05″ W. The site elevation is 1299 m above mean sea level and is located about 15 km west of Granite Mountain on the salt flats of the Great Salt Lake Desert. The geographical region of the site is a barren lake bottom (i.e., previously the floor of Lake Bonneville) consisting of a mixed clay, mud, and salt soil content that forms a very thin salt-laden crust over a naturally high water table. The average roughness length, z_0, is estimated to be approximately 1×10^{-4} m. The site is extremely flat (e.g., the terrain elevation varies by less than about 1 m over horizontal distances of about 10 km), hydraulically smooth, and spatially homogeneous with an unobstructed upwind fetch of more than 70 km in a wide sector. This area was selected with the objective of obtaining an observational site characterized by terrain as flat as practically achievable. Ideally, wind fluctuations over such flat terrain should be horizontally homogeneous.

The tracer used was propylene (C_3H_6). In each experiment, a finite mass of propylene gas was released nearly instantaneously (viz., the release time was $\lesssim 0.5$ s) from a special puff dissemination system, which consisted of an Air Blaster Model ABS-4-2 air cannon with an electrically activated control. The air cannon consisted of one or more cylinders of pressurized propylene, a quick-acting poppet valve, a solenoid fill-and-release control valve, and a high-volume exhaust valve. When activated, the air cannon discharged a user-selected quantity, say Q (nominally 0.35 kg per cannon), of gas. The velocity of the gas at the throat of the exhaust valve was equal to the local sonic velocity (i.e., a choked gas flow). The gas flow, directed vertical upwards from the cannon, impinged on a horizontal circular deflector plate placed above it. The height of the plate above the gas flow was used to regulate the height of the puff release, and the plate was used to deflect

102-02549/

the gas flow to form a nearly instantaneous cylindrical cloud of propylene gas with a diameter of approximately 2 m. A computer-controlled gas release system was incorporated with the air cannon to enable the system to operate in a periodic cycle. The poppet valve would open at pre-specified and regular times (e.g., on-times) to produce a quasi-instantaneous puff release and the air cannon would fill with propylene gas during the off-times. This dissemination mechanism can be used to produce a train of propylene puffs, thus enabling a number of replicates (repeat realizations) of the passive gas dispersion from the instantaneously released source to be measured.

The cloud concentrations were measured with fast-response photoionization detectors (DigiPid) that were manufactured commerically by S. & J. Engineering, Inc. (Richmond Hill, Ontario, Canada). This detector has a response time of about 0.02 s. The concentration time series corresponding to the puff-cloud passages through the sampling line were digitized with an 18-bit analog-to-digital (A/D) converter at a digitizing frequency of 50 Hz. Because instantaneous concentrations in a dispersing cloud typically span more than three decades in magnitude, a digital resolution of 18 bits is needed to define accurately the peak concentration values. The concentration detectors were calibrated regularly by placing them in a specially designed calibration unit mounted in a small rack. This unit consisted of 16 rectangular gas detector holders, a manifold for distributing the gas to each detector, and three mass flow controllers for controlling the flow rate and concentration of the calibration gas delivered to the detectors. In operation, up to five high-pressure calibration gas cylinders can be connected to the calibration unit with quick-connect fittings. In this study, the gas cylinders contained ultra-zero air and air with 10, 100, and 1000 parts per million (ppm) by volume propylene. The three mass flow controllers in the calibration unit were used to mix gas from the appropriate calibration gas cylinders with air to generate any desired gas concentration between 0 and 1000 ppm. The detectors were calibrated regularly over their entire operating range using reference concentrations of 0, 5, 10.2, 50, 110, 200, and 400 ppm propylene in air. A least-squares regression fit of the calibration data to a second-order polynomial, $\chi = a_0 + a_1 V + a_2 V^2$, provided an overall calibration for each detector, where V is the A/D output of the detector, χ is the absolute propylene concentration (ppm), and a_j ($j = 0, 1, 2$) are fitted calibration constants. Generally, the voltage output of the detectors was found to vary linearly with the propylene concentration in the range between 0 and about 50 ppm, and to exhibit a small to moderate concave downwards curvature at the higher concentration levels. However, a second-order polynomial was found to provide an accurate representation (to within ±2%) for the calibration data over the entire operating range of the detectors.

In addition to the concentration measurements, both standard and micrometeorological data were collected during the field experiments. Surface wind speed and direction were measured at 2 m above the ground with standard R. M. Young propeller anemometers and vanes mounted on tripods. Solar irradiation

(both incoming and outgoing long- and short-wave radiation) and air temperature were measured, respectively, with a pyranometer/actinometer sensor system and a fiberoptic-quartz thermometer. Upper level winds and temperatures were obtained from radiosonde, tethersonde, and pilot balloon (pibal) soundings that were made every 60 to 90 minutes during each test day. The horizonal (u, v) and vertical (w) components of the instantaneous wind velocity were measured with two- and three-axis sonic anemometers/thermometers (models RSWS-201/2A and RSWS-201/3A, Applied Technologies, Inc.) mounted on two 9-m meteorological masts at various levels between 1 and 8 m above the surface. Three-axis sonic anemometers/thermometers were installed at the 2- and 8-m levels and two-axis anemometers/thermometers were placed at the 0.5-, 1-, and 4-m levels on each of the two meteorological masts. The sonic anemometers/thermometers were oriented to true north to take advantage of prevailing winds within the north-west to north-east sectors. The sonic anemometer data were recorded at 10 Hz.

The propylene puffs were released at a height, z_s, of about 1.3 m (height of the centre of the initial source puff) and measured by concentration detectors at a height, z_d, of 1.6 m. A series of tracer experiments on concentration fluctuations in dispersing puffs were conducted over downwind distances of between 200 and 1200 m. The 48 detectors that were available for each experiment were arranged in a straight line roughly perpendicular to the mean wind direction with a crosswind extent of 282, 376, or 470 m (which correspond, respectively, to a 6-, 8-, or 10-m spacing between detectors). The sampling line was oriented in the east-west direction to take advantage of the typical northerly winds presiding at the site. Wind speed and direction measured by the propeller-vane anemometer were closely monitored, and when favourable conditions seemed imminent (e.g., the mean wind direction was approximately perpendicular to the sampling line of detectors), a puff was discharged from the air cannon and the samplers began data acquisition. In view of the fact that the instantaneous wind direction in which a particular puff is imbedded is not controllable or predictable, the crosswind extent of the sampling line (and the concomitant spacing of the detectors on the line) was chosen in the hope that at least six or more detectors measured the passage of each propylene cloud so as to provide a horizontal cross-section through the cloud and ensure that one detector was close to the cloud centroid given the expected variability in the wind azimuth during the particular field experiment. The spacing of the detectors was chosen to allow the investigation of instantaneous crosswind puff structure and define the instantaneous cross-puff dimensions.

3. Data Analysis Procedures

3.1. Initial Data Processing

Prior to performing data analysis, some preprocessing of the puff concentration time series is necessary. The initial processing of the raw concentration time series consists of four steps: (1) drift correction to the baseline level of the concentration time series to remove any slow variations (trends) in this level over the sampling time of the field experiment; (2) conversion of the concentration time series (in A/D units) to absolute concentration in parts per million by volume; (3) selection of an appropriate concentration threshold that will be used to distinguish a real concentration signal from instrumental noise on the baseline; and, (4) thresholding the concentration signal. The particular details of this procedure are briefly described below.

The baseline drift was removed by least-squares fitting cubic splines to the mean levels of the noise baseline segments between the concentration puff events and then subtracting the resulting curve from the recorded time series. Next, the resulting time series (in A/D units) was converted to absolute concentration (ppm) by applying the appropriate calibration curve (modelled as a second-degree polynomial) to the data. Following baseline and calibration corrections, a concentration threshold χ_T required to distinguish real concentration signals from the (level) noise baseline was determined from an analysis of the background concentration time series obtained before and after each dispersion experiment with the puff source turned off. In this study, a threshold of three standard deviations of the background noise level was used to define the nominal zero concentration level. With the selection of χ_T, the final stage of the initial data processing consisted of removal of the noise on the baseline by subtracting the concentration threshold from each data point in the concentration time series, taking care to ensure a non-negative result (i.e., all concentration values that become negative after subtraction of the threshold value are clipped to zero).

Following this preprocessing, it was necessary to identify the arrival and departure times of each instantaneous (non-zero) concentration-time profile of every puff sampled by the detectors anywhere along the crosswind sampling line. The arrival and departure times of the concentration-time profiles were obtained by a visual inspection of the concentration puff events recorded at each detector, and these times were then cross-referenced to the release time of a particular source release event. The concentration-time profiles associated with a particular source release can be used to prepare the distribution of puff instantaneous concentration as a function of time, t, and crosswind position, y, at a fixed downwind distance, x, from the source and at a fixed height, z, above the ground.

3.2. ENSEMBLE DEFINITION

Before the data analysis can proceed, it is necessary to define precisely the set of possible and admissible realizations (i.e., the ensemble) of puff-cloud passages on which the statistical description will be based. It should be emphasized that the statistical description of the phenomenon is useful only when the ensemble to which it applies is explicitly specified (viz., the statistical properties of the puff concentration field depend on the choice of the ensemble to which it refers). One possibility of such an ensemble is the set of puff concentration distributions measured relative to the instantaneous centres-of-mass of the puffs. Ensembles of puff concentration distributions measured in this way encapsulate the effects of relative diffusion. In this framework, the statistical properties of the instantaneous puff concentration field are determined by eddies with length scales similar to or less than the instantaneous cloud size, which act, respectively, to break up the cloud by entraining clean air and to mix the contaminant within the cloud with the entrained air.

In this paper, we concern ourselves with the analysis of the puff concentration data in the framework of relative diffusion. In this framework, the ensemble averages derived from the set of realizations of puff-cloud passages across the horizontal sampling line are evaluated only after the centres-of-mass of all the realizations have been made coincident. To this purpose, the definition of the ensemble in the framework of relative diffusion requires the determination of the centre-of-mass of each realization of the puff-cloud passage through the crosswind sampling line. Denote by y the horizontal distance measured along the crosswind sampling line from some fixed (but otherwise arbitrary) origin. For each puff-cloud passage across the sampling line, digitized records of the instantaneous puff concentration-time profiles, $\chi(y, t)$, are available as a function of y from the set of detectors that intercepted the dispersing puff. Because relative diffusion is being studied, the origin of y and t is chosen to be the centre-of-mass in the (t, y) plane. Hence, for the j-th puff-cloud concentration passage through the sampling line, the centre-of-mass in the (t, y) plane is defined by

$$t_C^{(j)} \equiv \iint t\chi^{(j)}(y, t)\, dt\, dy \Big/ \iint \chi^{(j)}(y, t)\, dt\, dy, \tag{1a}$$

and

$$y_C^{(j)} \equiv \iint y\chi^{(j)}(y, t)\, dt\, dy \Big/ \iint \chi^{(j)}(y, t)\, dt\, dy, \tag{1b}$$

where $\chi^{(j)}(y, t)$ is the j-th realization of the distribution of puff tracer concentration with respect to t and y. The position of the instantaneous centre-of-mass of the j-th cloud in the (t, y) plane, which will vary from realization to realization, is given by $(t_C^{(j)}, y_C^{(j)})$.

3.3. ENSEMBLE CONSTRUCTION

The puff events that are used to construct a particular ensemble in the framework of relative diffusion are carefully selected. All realizations (puff events) assigned to a particular ensemble must first satisfy the constraint that they be released from the same source location relative to the sampling line. In particular, clouds released from different downwind distances cannot belong to the same ensemble. Hence, the first step in the ensemble construction was to identify all cloud realizations released from a fixed source position, and then to nominally assign puff realizations measured over a continuous sampling period at that source position to various ensembles, using a preliminary visual inspection of the gross puff structure. Hence, all the realizations in a particular ensemble were selected from puff release events that were conducted close in time. Next, the wind velocity and temperature time series measured by the three-axis sonic anemometer/thermometer at the 2-m level were extracted for the time periods associated with each of these nominal ensembles. It should be noted that temperature was obtained from the speed of sound measurements made by the sonic anemometer/thermometer. Because the release conditions at the source were kept constant (approximately or better), in order to determine whether a particular instantaneous puff in a sequence of replications belongs to a given ensemble, it is necessary to ascertain whether the atmospheric conditions responsible for the puff dispersion were the same as, or similar to, those responsible for dispersion of the other puff realizations in the ensemble. Hence, the final step in the ensemble construction concerns the assessment of the turbulent wind and temperature fluctuations over the time period of the ensemble for stationarity.

A procedure was devised for this purpose, after considerable development. Firstly, the wind velocity and temperature time series were high-pass filtered to remove the mean variations and long-term trends from the data. The purpose of this step was to isolate only the eddy scales that are responsible for the in-cloud dispersion (e.g., the scales that determine primarily the relative diffusion of the cloud, and exclude scales responsible for the cloud meander). The high-pass filtering was implemented using a digital fourth-order Butterworth filter that was applied twice to the time series, once in the forward direction and once in the backward direction, in order to eliminate phase distortion. A common lower cutoff frequency was used to filter all the velocity and temperature time series. This high-pass filter cutoff frequency was chosen to be around 0.00167 Hz, which corresponds to a maximum allowable averaging time of 600 s. This value was chosen partly subjectively and partly after inspection of some selected puff dispersion events corresponding to the longest transport range ($\approx$ 1 km) measured in our field experiments.

Secondly, the high-pass filtered wind velocity and temperature time series were divided into non-overlapping segments corresponding to the interval between consecutive puff releases. An individual puff realization assigned to a given ensemble corresponds to one of these intervals (or, puff periods), and the wind velocity and

temperature data in each of these intervals may be considered to be independent (approximately or better).

Thirdly, several turbulence statistics for each puff period were computed: the velocity variances, $\left(\overline{u'^2}\right)_i$, $\left(\overline{v'^2}\right)_i$, and $\left(\overline{w'^2}\right)_i$ in the x-, y-, and z-directions; the Reynolds stresses (momentum fluxes), $\left(\overline{u'w'}\right)_i$ and $\left(\overline{v'w'}\right)_i$; and, the kinematic sensible heat flux, $\left(\overline{w'T'}\right)_i$. Here, T denotes the sonic temperature, the subscript i refers to the i-th puff period, and the overline $\overline{(\cdot)}$ refers to a time average. Assume that the time series have been divided into M equal non-overlapping intervals (puff periods). The values in each of the following sequences $\{\xi_i\}_{i=1}^{M}$ ($\xi \equiv \overline{u'^2}$, $\overline{v'^2}$, $\overline{w'^2}$, $\overline{u'w'}$, $\overline{v'w'}$, $\overline{w'T'}$) were aligned into a time sequence and assessed for stationarity by testing for the presence of trends or variations other than those due to expected sampling variations. The extent of similarity in the conditions corresponding to each puff interval of an ensemble is embodied in the sequences $\{\xi_i\}_{i=1}^{M}$. For similarity, it is required that the values of ξ_i do not vary significantly from one interval to the next, where the word 'significantly' here is used to refer to variations that are greater than would be expected due to statistical sampling variations. To test for the significance of these variations, we define the random variable $S \equiv \#\{(\xi_i - \xi_j) > 0, i < j\}$ associated with the number of sign changes in the sequence $\{\xi_i\}_{i=1}^{M}$. If $\{\xi_i\}_{i=1}^{M}$ is derived from a stationary process, then the variations of S (sign changes in the original sequence of sampled values ξ_i) will be random and display no trends. Now, for $M \gtrsim 10$, S will be expected to be approximately normal with mean $M(M-1)/4$ and variance $M(M-1)(2M+5)/72$ (Kendall and Stuart, 1977). The hypothesis of stationarity of the wind velocity and temperature time series relative to the turbulence statistic ξ is tested by comparing the observed difference between S and $M(M-1)/4$ (e.g., expected value for S assuming stationarity in the underlying time series) with the difference that would be expected due to statistical variability in S. The acceptance region for the hypothesis test at any desired level of significance α is given by

$$z_{\alpha/2} \leq \frac{S - M(M-1)/4}{\sqrt{M(M-1)(2M+5)/72}} \leq z_{1-\alpha/2},$$

where z_α denotes the 100α percentage point for a standard normal or Gaussian distribution (or, equivalently, the normal quantile of order α). For the current study, the hypothesis test was applied with $\alpha = 0.1$; viz., the probability of rejecting the hypothesis when it is true is 0.1. It should be stressed that the test for stationarity described here only verifies weak stationarity in the background turbulence (e.g., time invariance of the velocity variances and momentum fluxes). Proof of strict stationarity in the background turbulence would not be feasible in practical terms because this will involve verification that all the statistical properties of the turbulence are invariant with respect to time translations.

Following the procedure described above, we constructed 17 ensembles of puff realizations. All these ensembles passed the simple test of weak stationarity for

TABLE I

Summary of principal variables for puff-cloud ensembles. Here, x is the downwind distance (i.e., distance from the source location to the geometric centre of the horizontal sampling line); Q is the average mass of material released in each concentration puff; n is the number of puff realizations assigned to the ensemble; and, U_T is the overall (global) mean cloud transport speed for the puff realizations in the ensemble (cf. Section 3.4 for further details)

Ensemble	x (m)	Q (kg)	n	U_T (m s^{-1})
R01	192	0.37	20	6.92
R02	192	0.36	11	7.03
R03	192	0.36	29	5.77
R04	299	0.36	24	3.63
R05	354	0.73	18	3.74
R06	354	0.73	17	2.27
R07	354	0.73	19	3.24
R08	354	0.74	31	4.15
R09	354	0.75	31	4.33
R10	800	0.74	12	3.24
R11	800	1.42	31	7.40
R12	800	1.33	20	6.81
R13	800	1.35	35	4.98
R14	800	1.34	22	3.91
R15	800	1.33	12	2.86
R16	1200	2.35	22	7.22
R17	1200	1.80	19	5.54

the small set of background turbulence statistics considered (e.g., velocity variances, momentum fluxes). Table I provides a list of important variables for these ensembles. A compendium of turbulence statistics data for the averaging periods associated with the 17 ensembles is given in Table II. All the turbulence statistics for each ensemble were determined from the associated sonic velocity time series over the entire sampling period associated with the ensemble, viz., these statistics were not calculated as average values over the subintervals corresponding to the puff realizations in each ensemble. Here, wind components are calculated in a

TABLE II

Summary of turbulence statistics measured with a 3-axis sonic anemometer/thermometer at 2 m. Here U is mean wind speed; σ_u, σ_v, and σ_w are the standard deviations of velocity fluctuations in the alongwind, crosswind, and vertical directions, respectively; u_* is friction velocity; and, L is the Obukhov length

Ensemble	U ($m\,s^{-1}$)	σ_u ($m\,s^{-1}$)	σ_v ($m\,s^{-1}$)	σ_w ($m\,s^{-1}$)	u_* ($m\,s^{-1}$)	L (m)
R01	5.85	0.777	0.842	0.296	0.261	−18.1
R02	5.58	0.683	0.746	0.276	0.262	−36.4
R03	4.60	0.593	0.545	0.231	0.201	−78.6
R04	3.61	0.462	0.429	0.193	0.163	−20.4
R05	3.61	0.657	0.827	0.277	0.203	−4.42
R06	1.98	0.661	0.691	0.241	0.084	−0.4
R07	3.19	0.615	0.651	0.229	0.150	−3.26
R08	4.40	0.566	0.543	0.223	0.190	−17.6
R09	4.61	0.495	0.301	0.225	0.194	−207
R10	3.41	0.371	0.253	0.184	0.160	226
R11	7.38	0.886	0.692	0.360	0.342	−72.3
R12	6.87	0.953	0.865	0.117	0.303	−24.5
R13	4.54	0.801	0.755	0.258	0.214	−10.6
R14	3.69	0.489	0.427	0.198	0.177	−34.0
R15	2.65	0.315	0.211	0.136	0.110	74.3
R16	7.06	1.04	0.929	0.359	0.320	−20.6
R17	5.11	0.615	0.375	0.272	0.246	133

coordinate system with alongwind, crosswind, and vertical components denoted u, v, and w, respectively. The Obukhov length, L, was estimated as

$$L = -\frac{u_*^3 T}{\kappa g \overline{w'T'}}, \tag{2}$$

where u_* is the friction velocity at the surface, $\kappa \approx 0.4$ is the von Karman constant, and g is the acceleration due to gravity. The influence of the mean humidity flux on the value of L was considered to be negligible. A primed quantity is used to indicate a turbulent fluctuation. The friction velocity was estimated by

$$u_* = \left[\left(\overline{u'w'}\right)^2 + \left(\overline{v'w'}\right)^2\right]^{1/4}. \tag{3}$$

3.4. ENSEMBLE-AVERAGED CONCENTRATION STATISTICS

The evaluation of various ensemble-averages of the contaminant cloud concentration is undertaken after all realizations $\chi^{(j)}(y, t)$ in a given ensemble are translated so that their centres-of-mass in the (t, y) plane are made to coincide, and the puff "lengths" (durations) in the t-direction are dilated (or, contracted) by the local cloud transport speed, $U_T^{(j)}$, for the j-th realization. The cloud transport speed, $U_T^{(j)}$, of the j-th puff realization is determined as follows. For the j-th puff in an ensemble, denote by $r^{(j)}$ the Euclidean distance between the source position and the crosswind location of the puff centre-of-mass, $y_C^{(j)}$, [cf. Equation (1b)] along the horizontal sampling line at the downwind distance x. The local transport speed is determined as $U_T^{(j)} = r^{(j)}/t_C^{(j)}$, where $t_C^{(j)}$ is defined in Equation (1a).

In detail, let us first define the relative coordinates using the centre-of-mass positions, $t_C^{(j)}$ and $y_C^{(j)}$, as embodied in Equations (1a) and (1b):

$$t_r \equiv t - t_C^{(j)}, \tag{4a}$$

and

$$y_r \equiv y - y_C^{(j)}, \tag{4b}$$

so that the origin of t_r and y_r is, for each realization, chosen to be the centre-of-mass of the instantaneous puff in the (t, y) plane. Next, translate and dilate the j-th puff concentration realization to give the distribution of concentration in the framework of relative diffusion:

$$\chi_r^{(j)}(y_r, t_r) = \chi^{(j)}\left(y_r + y_C^{(j)}, (t_r + t_C^{(j)})\frac{U_T^{(j)}}{U_T}\right),$$

where U_T is the overall (global) cloud transport speed for all the puff realizations in the ensemble, viz., $U_T \equiv n^{-1}\sum_{j=1}^{n} U_T^{(j)}$, where n is the number of realizations comprising the ensemble. It is possible for the calculated lateral centroid, $y_C^{(j)}$, to occur between the positions of the detectors along the sampling line. In this case, $y_C^{(j)}$ for the j-th puff realization is simply rounded up to the nearest detector position. No attempts were made to interpolate $\chi_r^{(j)}(y_r, t_r)$ in y_r for the purpose of constructing the various ensemble averages described below.

We can now determine the ensemble average of any function or functional, $\psi(\chi_r)$, of the relative puff concentration $\chi_r(y_r, t_r)$. The ensemble average, $\langle\psi\rangle_n$, of ψ given a total number n of realizations in the ensemble is defined by

$$\left\langle\psi\left(\chi_r(y_r, t_r)\right)\right\rangle_n \equiv \frac{1}{n}\sum_{j=1}^{n}\psi\left(\chi_r^{(j)}(y_r, t_r)\right). \tag{5}$$

Obviously, the ensemble average $\langle\psi\rangle_n$ is an estimate of the mean value (expected value or mathematical expectation) because, for any n, $\mathbf{E}(\langle\psi\rangle_n) = \mathbf{E}(\psi) \equiv \langle\psi\rangle$. Furthermore, it can be demonstrated (Parzen, 1960) that $\langle\psi\rangle_n$ tends to $\langle\psi\rangle$ almost certainly (i.e., with probability one) as n tends to infinity, and that the error in using $\langle\psi\rangle_n$ to approximate $\langle\psi\rangle$ (for sufficiently large n) is proportional to the standard deviation of ψ and decreases as the square root of n (i.e., n must be quadrupled to halve the error).

As an example of the specific application of Equation (5), the ensemble averages of the power functions of χ_r [i.e., $\psi(\chi_r) \equiv \chi_r^p$] are simply the concentration moments; hence, the ensemble average of $\chi_r^p(y_r, t_r)$ yields the p-th order concentration moment at crosswind position y_r and time t_r. In particular, the ensemble-mean concentration $C(y_r, t_r)$ is defined by [$\psi(\chi_r) \equiv \chi_r$]

$$C(y_r, t_r) \equiv \langle\chi_r(y_r, t_r)\rangle_n = \frac{1}{n}\sum_{j=1}^{n} \chi_r^{(j)}(y_r, t_r); \tag{6a}$$

and, the concentration variance is determined by [$\psi(\chi_r) \equiv (\chi_r - C)^2$]

$$\sigma_c^2(y_r, t_r) \equiv \langle\chi_r'^2(y_r, t_r)\rangle_n = \frac{1}{n}\sum_{j=1}^{n}\left(\chi_r^{(j)}(y_r, t_r) - C(y_r, t_r)\right)^2. \tag{6b}$$

Similarly, the ensemble-mean dosage and dosage variance can be obtained, respectively, as follows:

$$D(y_r, t_r) \equiv \langle\mathcal{D}(y_r; t_r)\rangle_n = \frac{1}{n}\sum_{j=1}^{n} \mathcal{D}^{(j)}(y_r; t_r); \tag{7a}$$

and,

$$\sigma_D^2 \equiv \langle\mathcal{D}'^2(y_r; t_r)\rangle_n = \frac{1}{n}\sum_{j=1}^{n}\left(\mathcal{D}^{(j)}(y_r; t_r) - \langle\mathcal{D}(y_r; t_r)\rangle_n\right)^2, \tag{7b}$$

where $\mathcal{D}(y_r; t_r)$ is the functional of concentration (e.g., dosage or time-integral of instantaneous concentration) defined as follows:

$$\mathcal{D}(y_r; t_r) = \int_{-\infty}^{t_r} \chi_r(y_r, t)\, dt. \tag{8}$$

As $t_r \to \infty$, $\mathcal{D}$ becomes the total dosage, observable during the entire passage of a diffusing cloud.

It is interesting to note that the dosage variance is related to the concentration variance through the following relationship:

$$\langle \mathcal{D}'^2(t_r) \rangle = 2 \int_{-\infty}^{t_r} \langle \chi_r'^2(t) \rangle T_c(t)\, dt, \tag{9}$$

where

$$T_c(t) \equiv \int_{-\infty}^{t} \rho(\chi_r; t; \tau)\, d\tau, \tag{10}$$

is the integral time scale of concentration fluctuations. Here, $\rho(\chi_r; t, \tau)$ is the autocorrelation function of concentration fluctuations defined as follows:

$$\rho(\chi_r; t, \tau) = \frac{\langle \chi_r'(t) \chi_r'(\tau) \rangle}{\langle \chi_r'^2(t) \rangle}, \tag{11}$$

where t and τ are two diffusion times. To be strictly correct, it should be emphasized that $\rho(\chi_r; t, \tau)$ defined in Equation (11) is not a true correlation function in the sense that its denominator is not the product of two root-mean-squares (e.g., the denominator in the true correlation function would involve the product of the concentration standard deviations at times t and τ, rather than simply the concentration variance at time t). Because of this, $\rho(\chi_r; t, \tau)$ will not necessarily be less than unity in absolute magnitude. Note that, because the dispersion in an evolving cloud is not statistically stationary, the autocorrelation function for the cloud concentration must be a function of two diffusion times, namely t and τ [or, equivalently, of the diffusion time t and the lag time $(t - \tau)$]. The puff concentration realizations in a particular ensemble can be used to estimate the autocorrelation function of concentration fluctuations in accordance with Equation (11), and this quantity can subsequently be used to determine the integral time scale, $T_c(t)$, according to the prescription in Equation (10).

4. Results

4.1. Instantaneous concentration-time profiles

Typical examples of instantaneous concentration-time profiles in a dispersing cloud are presented in Figure 1. The origin of time t in these puff-cloud passages refers to the time measured from the arrival time of the 'waveform'. The waveforms exhibited in Figure 1 correspond to three independent concentration-time profiles, taken from Ensemble R09 near the instantaneous cloud centre-of-mass. The conditions were slightly unstable with a mean windspeed of 4.61 m s^{-1}.

The instantaneous concentration-time profiles appear to be highly irregular. There exist large local variations in concentration level resulting in steep gradients.

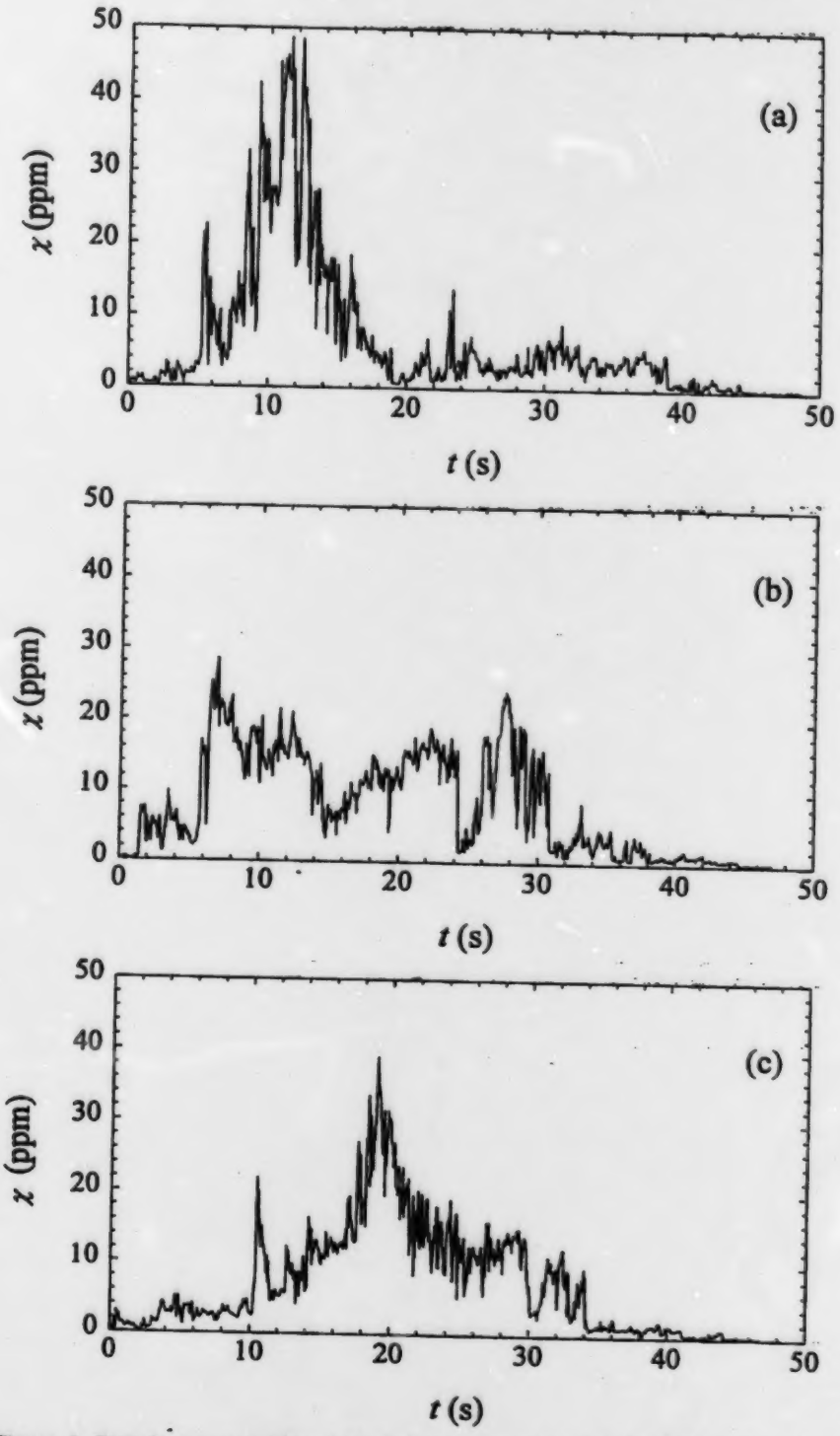

Figure 1. Sample concentration time series measured in 3 individual realizations near the cloud centre. The time series were obtained from Ensemble R09. Here, the elapsed time, t, refers to time measured from the arrival time of the puff.

The concentration traces are intermittent, exhibiting periods of low concentration with random duration interspersed with random short bursts of high concentration, suggesting that a wide range of time scales are responsible for the complex concentration-time profile patterns observed in Figure 1. Interestingly, low-concentration contaminant, or even unmixed (clean) ambient air, may be found in regions close to the cloud centre. The puff concentrations generally appear to decay away in long extended tails that also exhibit the fine structure of rapid fluctuations observed near the "core" of the cloud.

4.2. ENSEMBLE-AVERAGED PROFILES

Typical examples of ensemble averages of various functions and functionals of the instantaneous cloud concentration are illustrated in this section. The data for the examples shown here are taken from Ensemble R09. To simplify notation, t and y will henceforth be used to denote time and crosswind position in relative coordinates (viz., subscript r will be dropped).

Ensemble-mean concentration-time profiles, $C(y, t)$, measured at three different crosswind positions y in the dispersing cloud, are displayed in Figure 2. Similarly, lateral cross-sections of the ensemble-mean concentration are shown in Figure 3 at three different values of time t. The error bars shown in Figures 2 and 3 correspond to the standard deviation in the estimates of the ensemble-mean concentration for a finite sample size. Indeed, for the small number of puff realizations that are available for the construction of ensemble averages, it is expected that the sampling error will be a major source of uncertainty. We have applied the Bayes rule (Box and Tiao, 1973) to estimate the degree of uncertainty in our construction of the estimates for the ensemble-mean concentration and concentration variance (presented below) arising from the finite (and usually relatively small) sample size. Closed-form expressions for the variance (or, equivalently, the standard deviation) in the estimates for the ensemble-mean concentration and concentration variance have been derived using the Bayesian approach and used to provide "error bars" for these estimates. Furthermore, we note that the standard deviation in the estimates can be used in conjunction with Chebyshev's inequality (Parzen, 1960) to bound the probability of deviation of the ensemble-mean concentration or concentration variance estimates from their true (but unknown) values. However, it should be emphasized that these Bayes confidence intervals for the estimates of ensemble-mean concentration and concentration variance correspond to one-at-a-time confidence intervals where each point in the curve is treated individually, rather than simultaneous confidence intervals where all the points in the curve are treated simultaneously.

A comparison of Figure 1 with Figure 2 indicates that the ensemble-averaged concentration-time profiles are dramatically smoothed by the averaging procedure relative to the instantaneous concentration-time profiles. In particular, the ensemble-averaged concentration-time profiles are smeared out relative to the

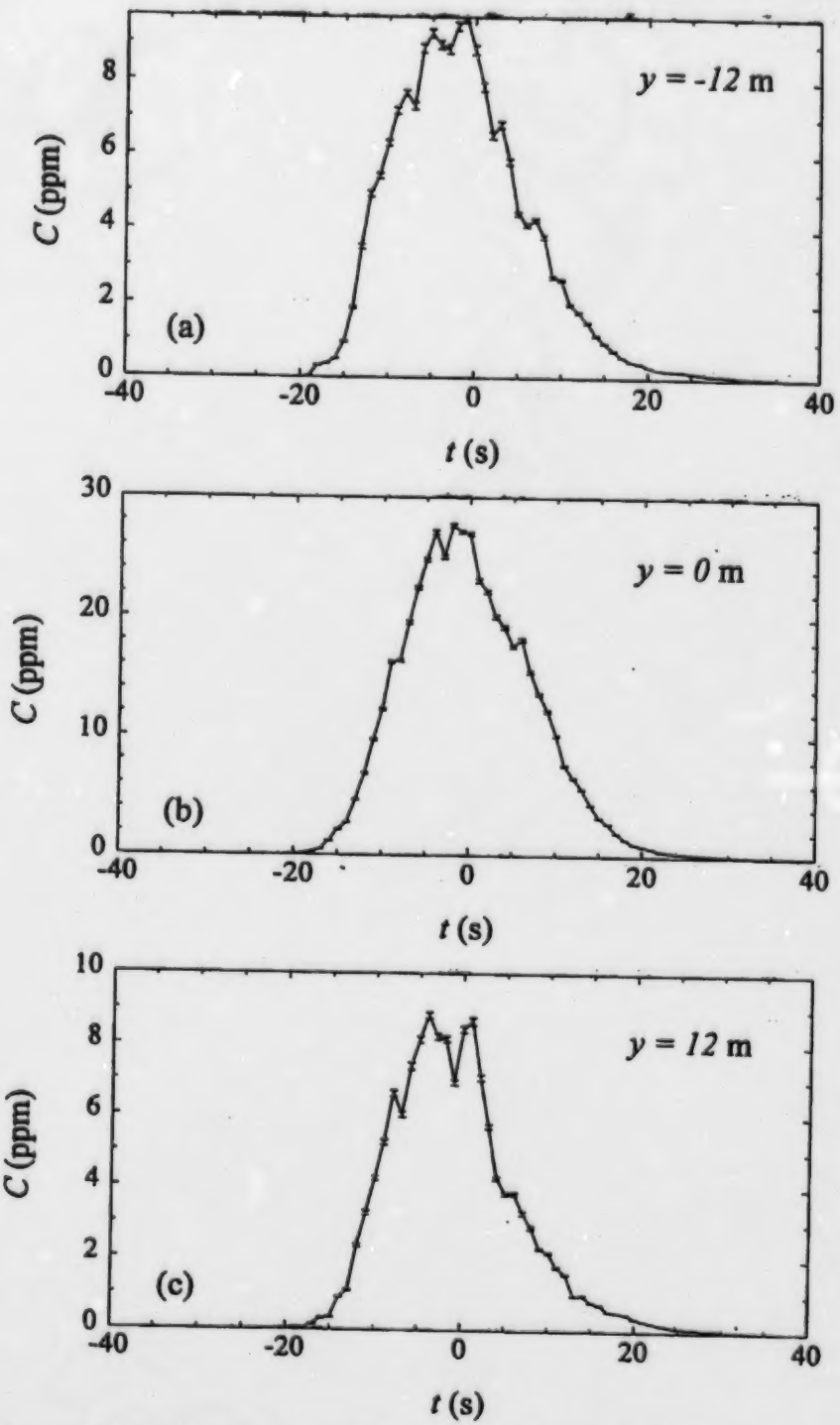

Figure 2. Ensemble-mean concentration-time profiles measured at 3 crosswind positions y in the cloud. The data were obtained from Ensemble R09. Vertical bars indicate the standard deviation in the estimate for the ensemble-mean concentration.

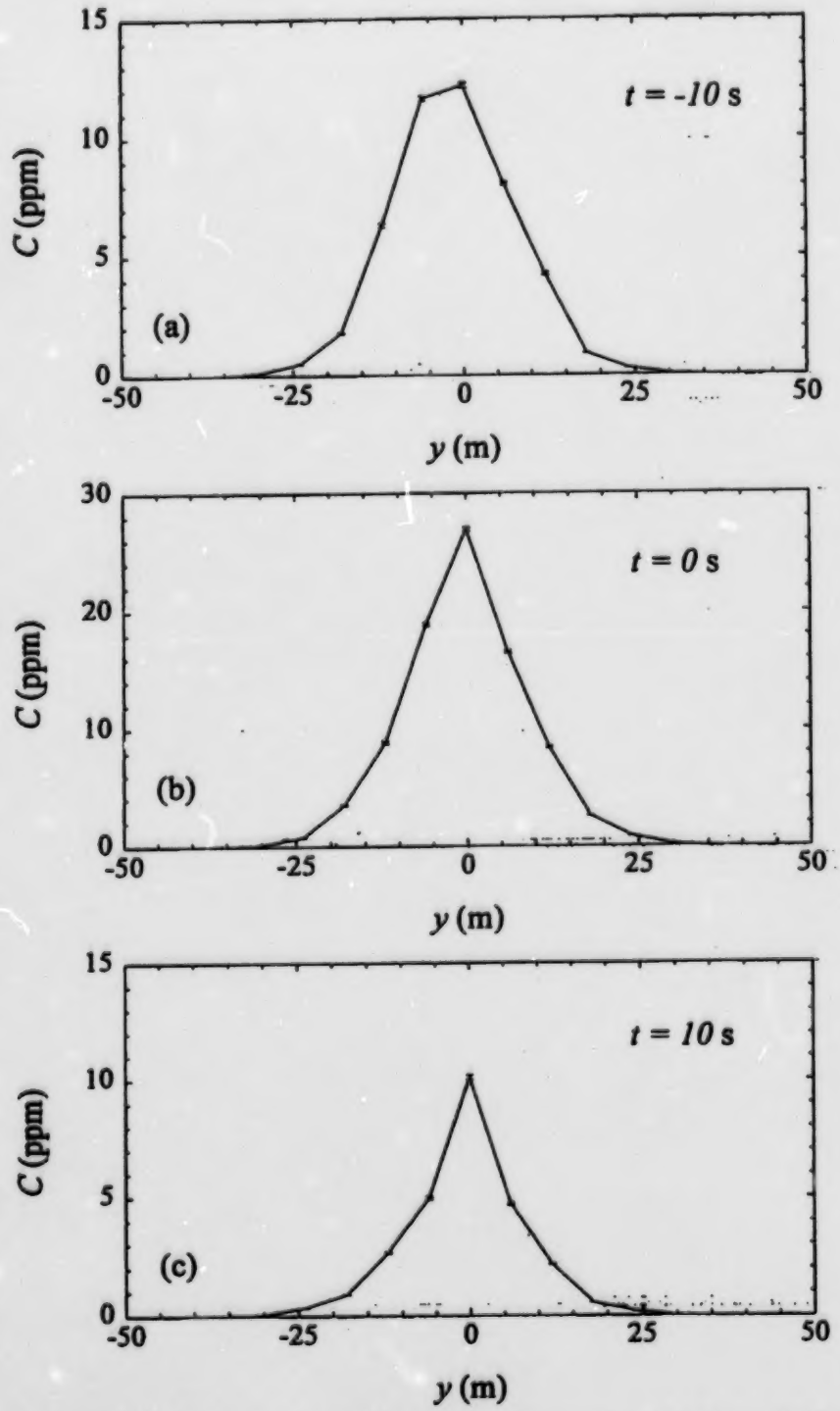

Figure 3. Lateral cross-sections of the ensemble-mean concentration measured at 3 diffusion times t in the cloud. The data were obtained from Ensemble R09. Vertical bars indicate the standard deviation in the estimate for the ensemble-mean concentration.

instantaneous ones, since the instantaneous concentration structures appear randomly in time with jitter in their size, shape, and amplitude. The ensemble-mean concentration-time profiles are decidedly non-Gaussian. They appear to be skewed to the right in the sense that the leading edge of the mean concentration profile rises more rapidly than the trailing edge (note the long tail region of decay), resulting in ensemble-averaged shapes that are decidedly non-symmetrical. In contrast, the crosswind profiles of ensemble-mean concentration shown in Figure 3 are symmetrical (approximately or better) and appear to be approximately a Gaussian function of y (at fixed t).

The concentration variance time profiles are presented in Figure 4 for three different values of y. Figure 5 shows lateral cross-sections of concentration variance σ_c^2 for three different values of t. The statistical error in the estimates of σ_c^2 are larger than those of C. In spite of the uncertainties in the estimates of σ_c^2, it nevertheless appears that the concentration variance time profiles and lateral cross-sections resemble the corresponding profiles for the ensemble-mean concentration in general overall shape. However, the concentration variance time profiles are shorter in duration (viz., decay more rapidly) than the ensemble-mean concentration-time profiles. Also, the crosswind dimension of the concentration variance lateral cross-section is smaller than that of the ensemble-mean concentration.

The time profiles and lateral cross-sections of concentration fluctuation intensity σ_c/C are displayed in Figures 6 and 7, respectively. An interesting observation is that $\sigma_c \approx C$ (viz., the variation about the ensemble-mean concentration is of the same order of magnitude as the mean concentration itself), even for instantaneous cloud concentrations measured in the framework of relative diffusion. The fluctuation intensity provides a measure of the degree of concentration fluctuations in the dispersing cloud, and in the framework of relative diffusion the magnitude of concentration variations observed in the cloud arises from entrainment of clean air into the cloud, which acts to break up the cloud, and from internal mixing of the contaminant within the cloud. Observe that the lateral cross-sections of fluctuation intensity are seen to increase towards the edges of the cloud from a minimum at the cloud centre-of-mass. Hence, the instantaneous cloud is not similar at all points in the cross-section.

Figures 8 and 9 show, respectively, three time profiles (at fixed lateral positions) and three crosswind distribution curves (at fixed times) for the ensemble-mean dosage, D. The ensemble-mean dosage time profiles exhibit a similar overall sigmoidal shape characterized by a steep rise at the leading cloud edge that flattens out at larger times corresponding to the trailing edge (cf. Figure 8). Lateral cross-sections of the ensemble-mean dosage are approximately symmetric and appear to be Gaussian in form (cf. Figure 9).

The time profiles and crosswind cross-sections of the dosage variance, σ_D^2, are displayed in Figures 10 and 11. Note that the σ_D^2 time profiles and lateral cross-sections have approximately the same shapes as those of D. It is of interest to

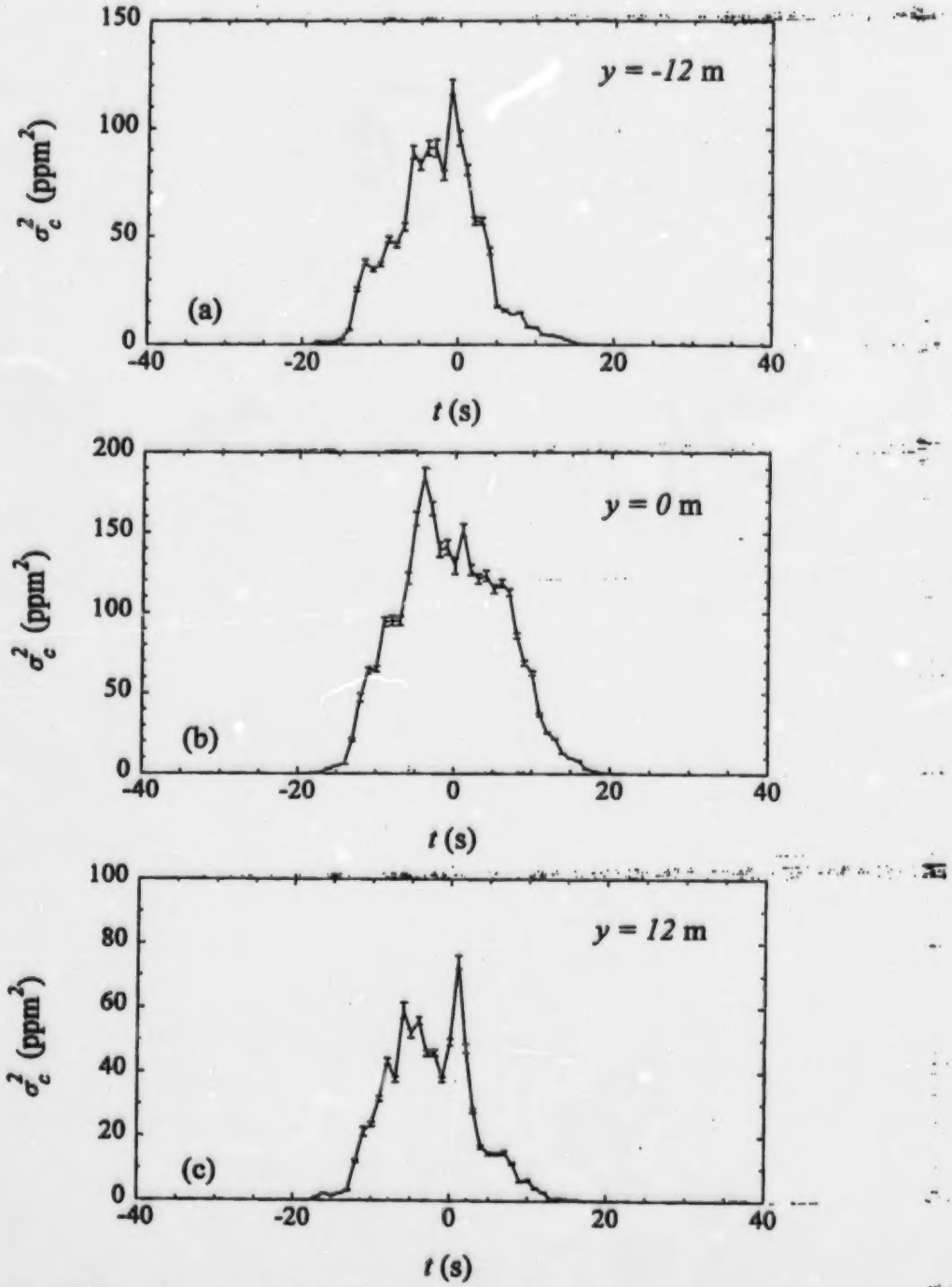

Figure 4. Concentration variance time profiles measured at 3 crosswind positions y in the cloud. The data were obtained from Ensemble R09. Vertical bars indicate the standard deviation in the estimate for the concentration variance.

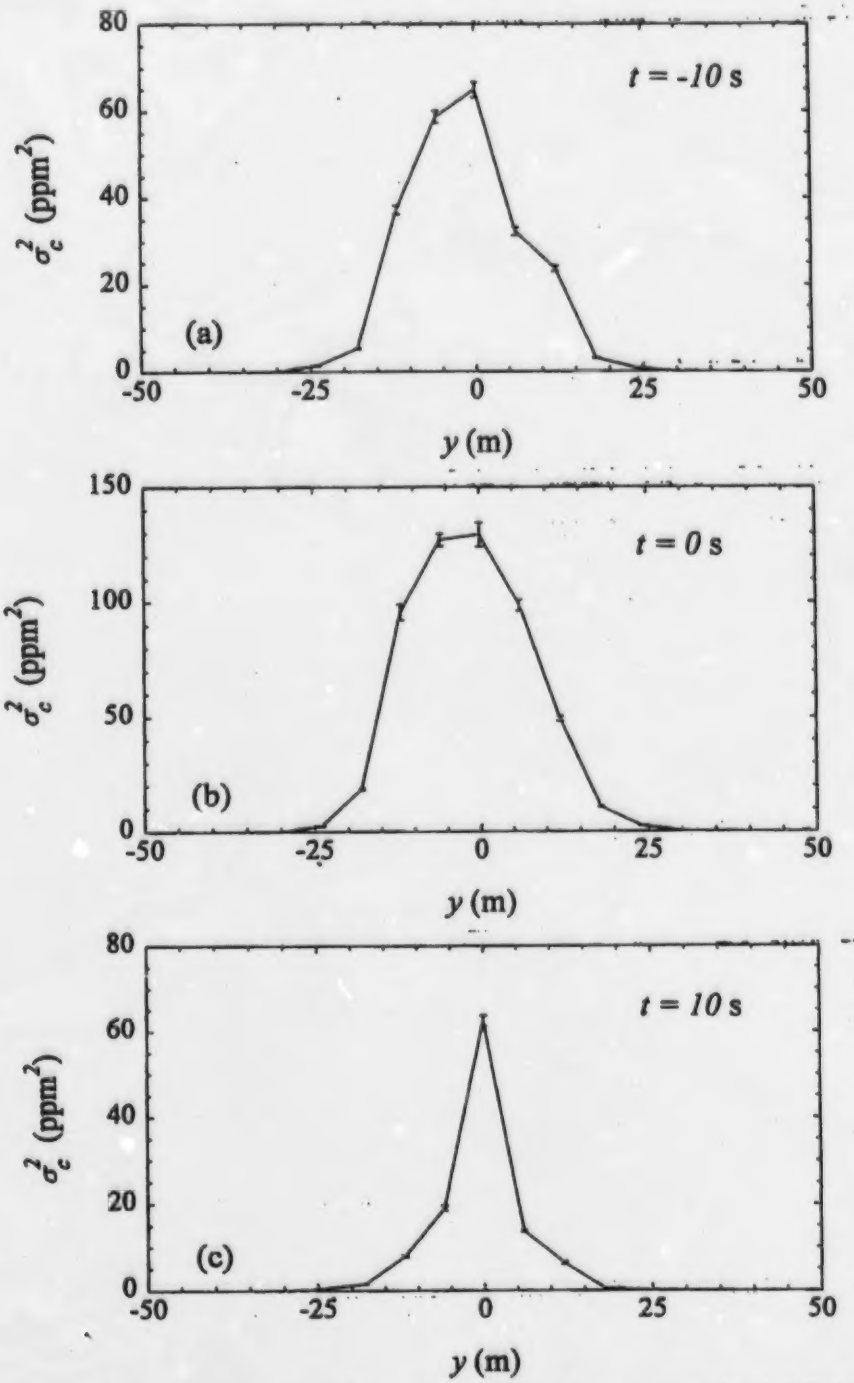

Figure 5. Lateral cross-sections of the concentration variance measured at 3 diffusion times t in the cloud. The data were obtained from Ensemble R09. Vertical bars indicate the standard deviation in the estimate for the concentration variance.

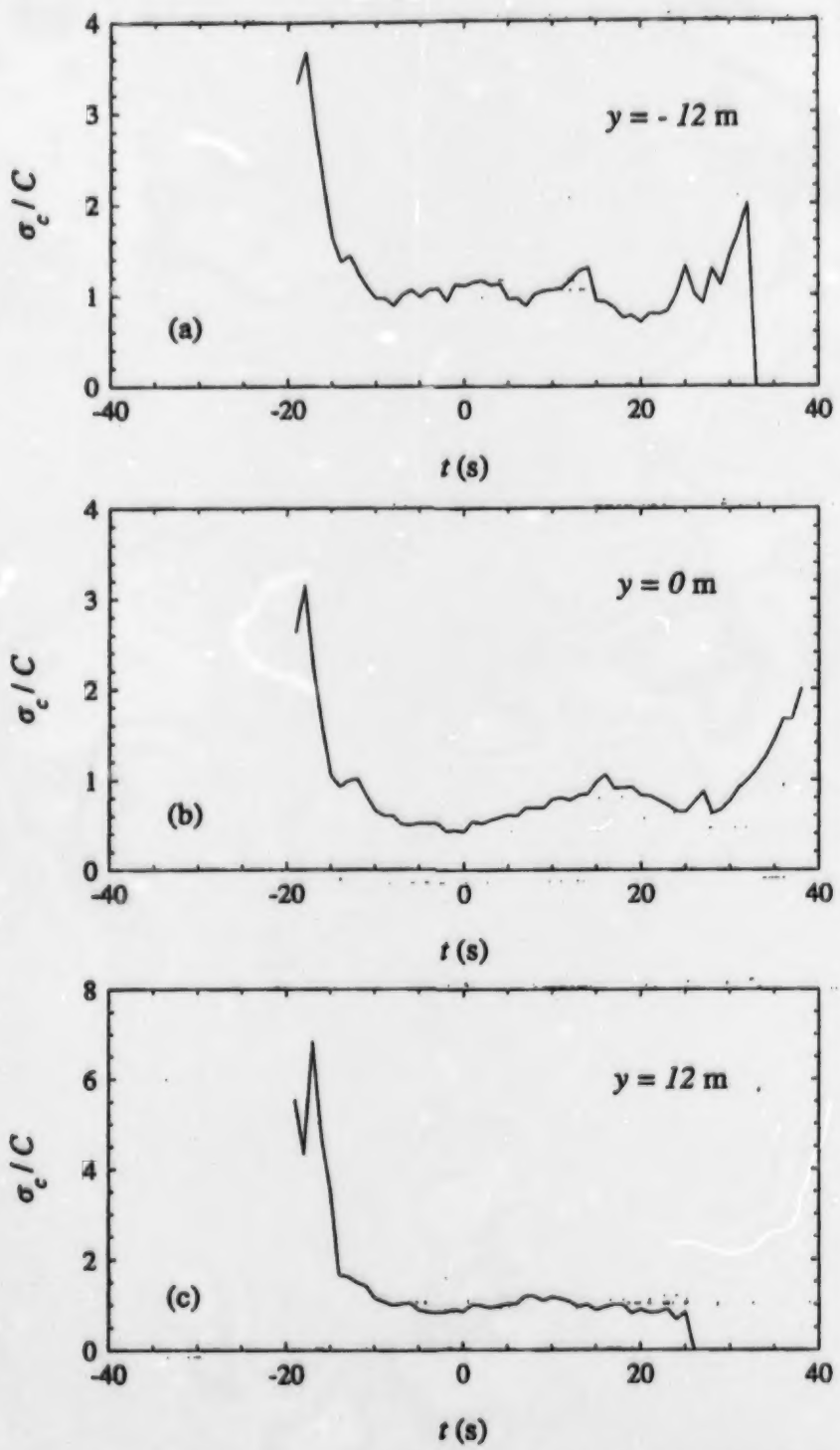

Figure 6. Time profiles of the concentration fluctuation intensity measured at 3 crosswind positions y in the cloud. The data were obtained from Ensemble R09.

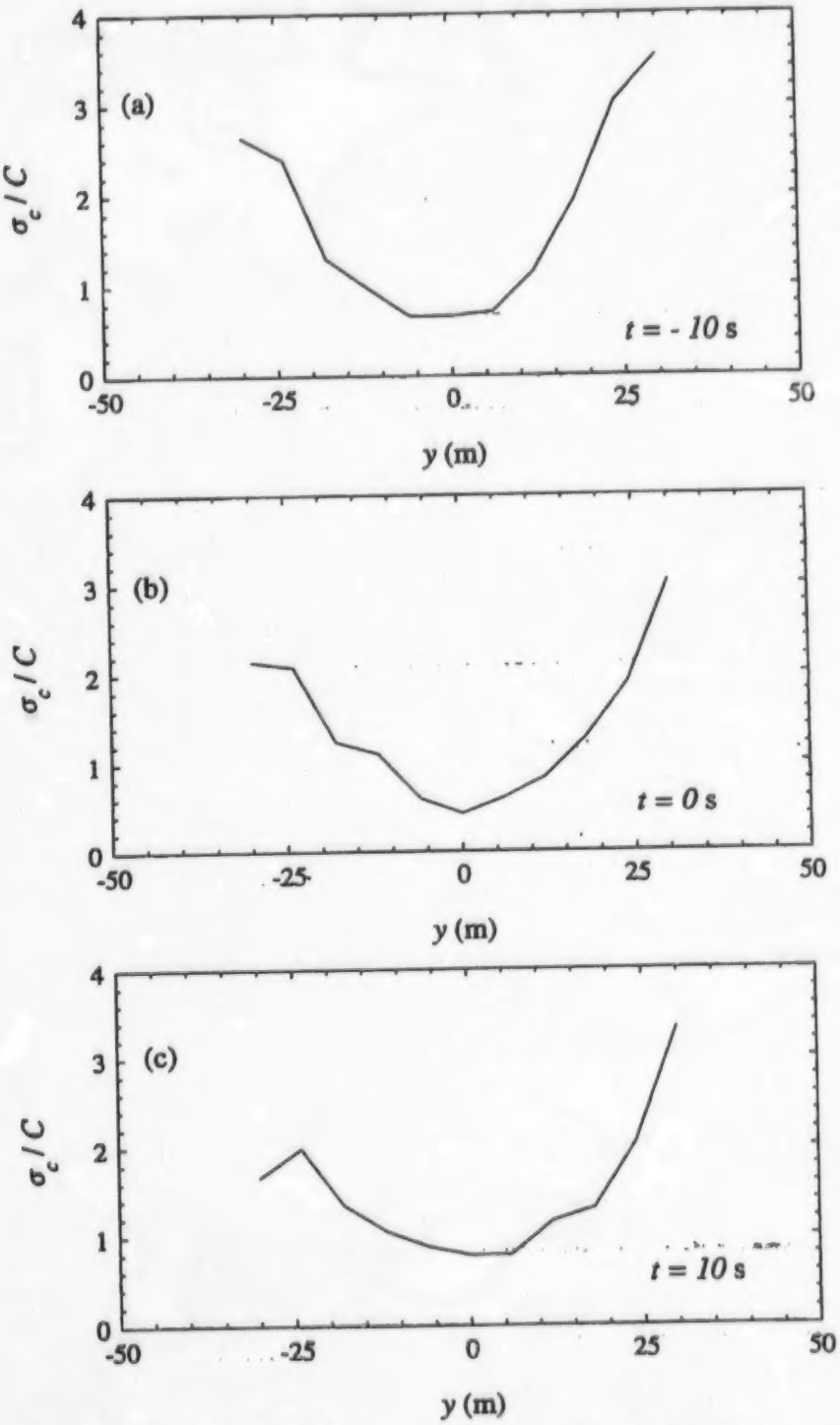

Figure 7. Lateral cross-sections of the concentration fluctuation intensity measured at 3 diffusion times t in the cloud. The data were obtained from Ensemble R09.

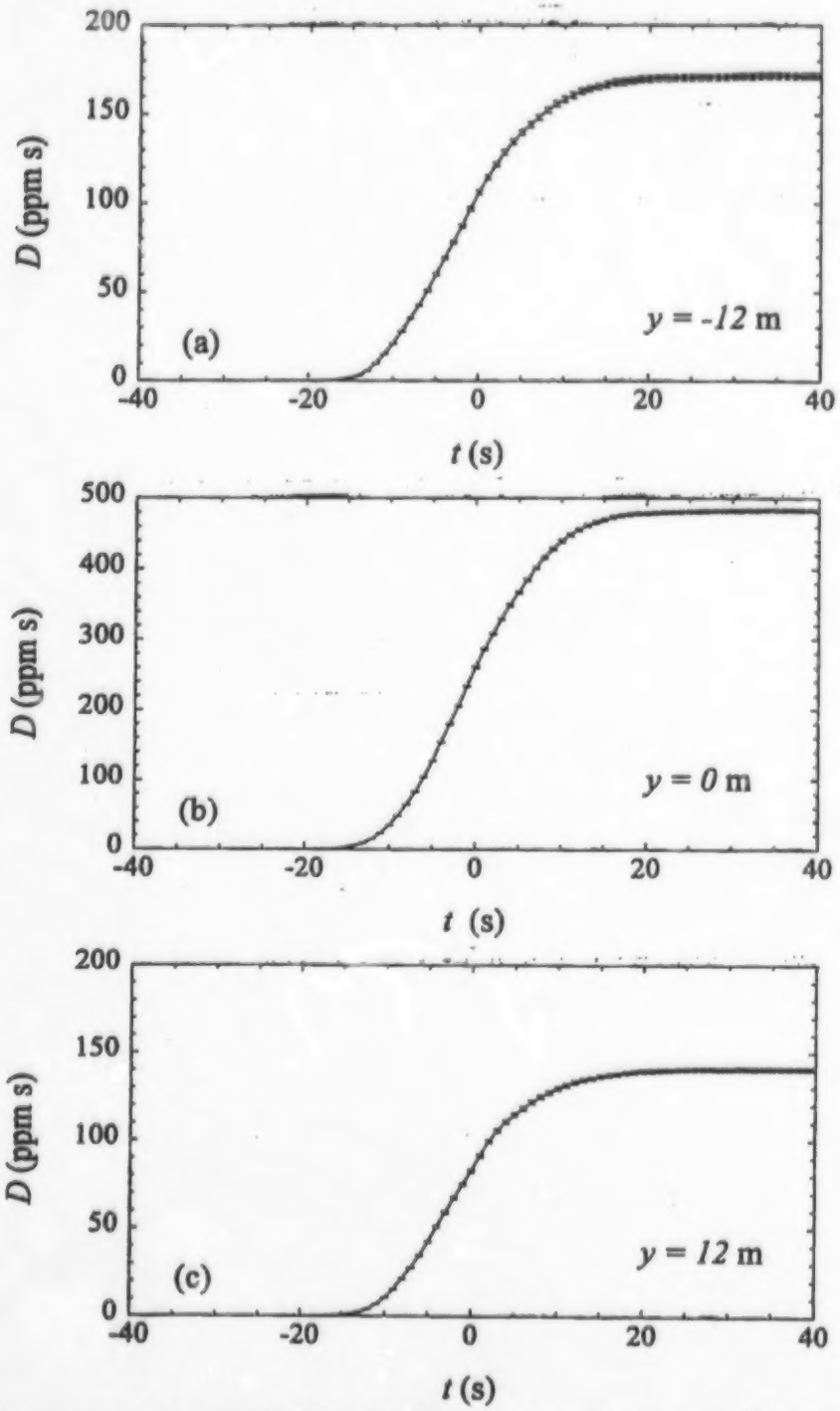

Figure 8. Ensemble-mean dosage time profiles measured at 3 crosswind positions y in the cloud. The data were obtained from Ensemble R09. Vertical bars indicate the standard deviation in the estimate for the ensemble-mean dosage.

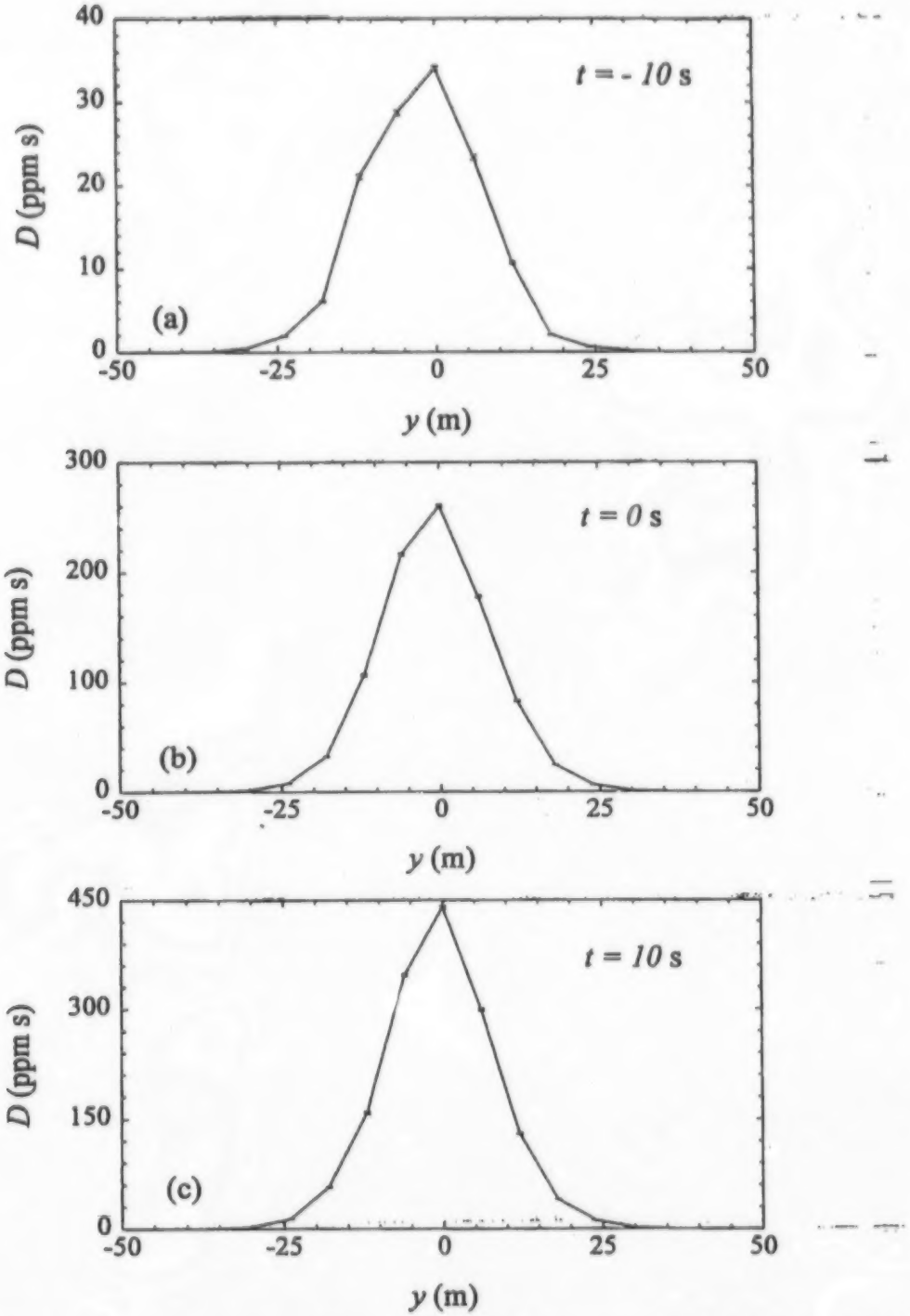

Figure 9. Lateral cross-sections of the ensemble-mean dosage measured at 3 diffusion times t in the cloud. The data were taken from Ensemble R09. Vertical bars indicate the standard deviation in the estimate for the ensemble-mean dosage.

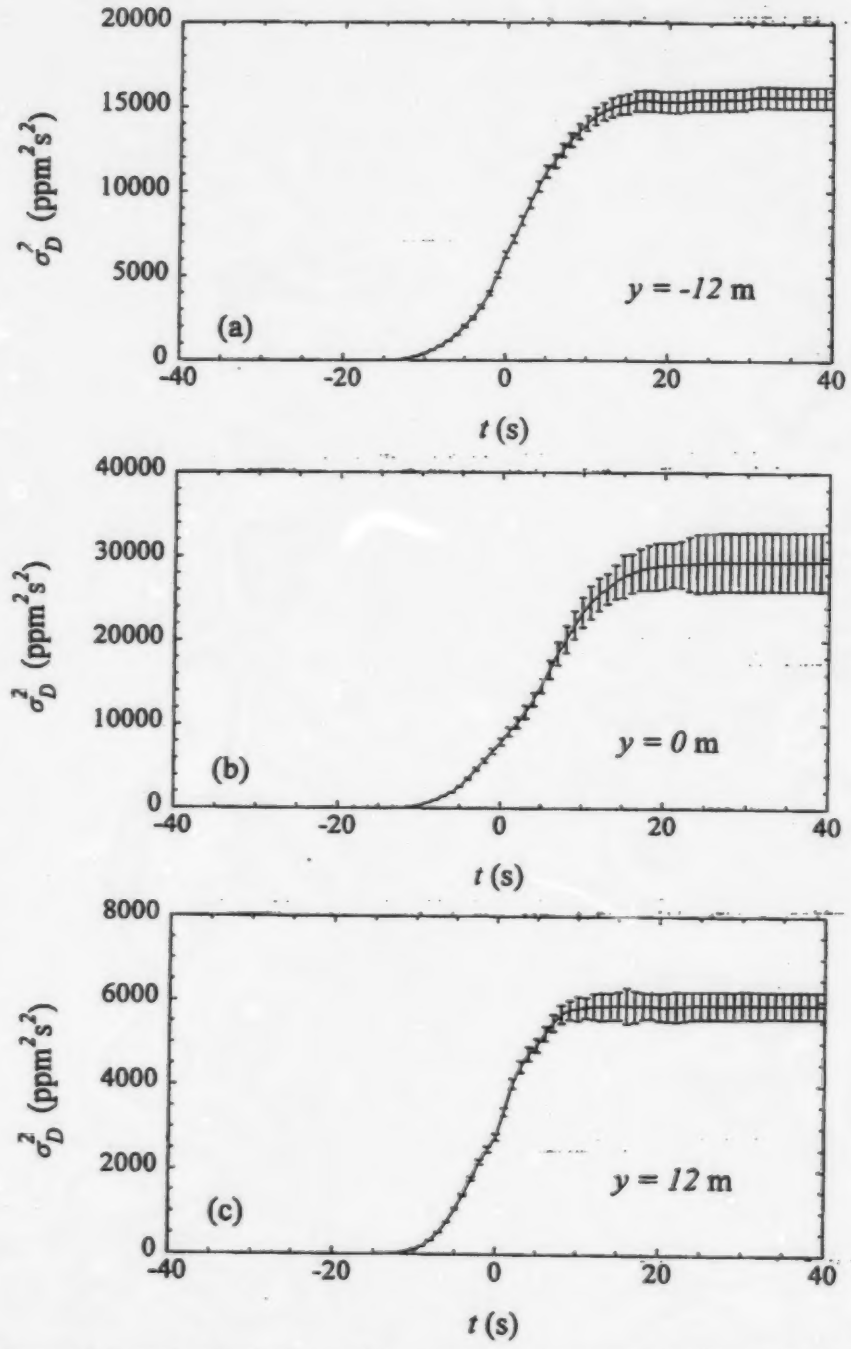

Figure 10. Dosage variance time profiles measured at 3 crosswind positions y in the cloud. The data were obtained from Ensemble R09. Vertical bars indicate the standard deviation in the estimate for the dosage variance.

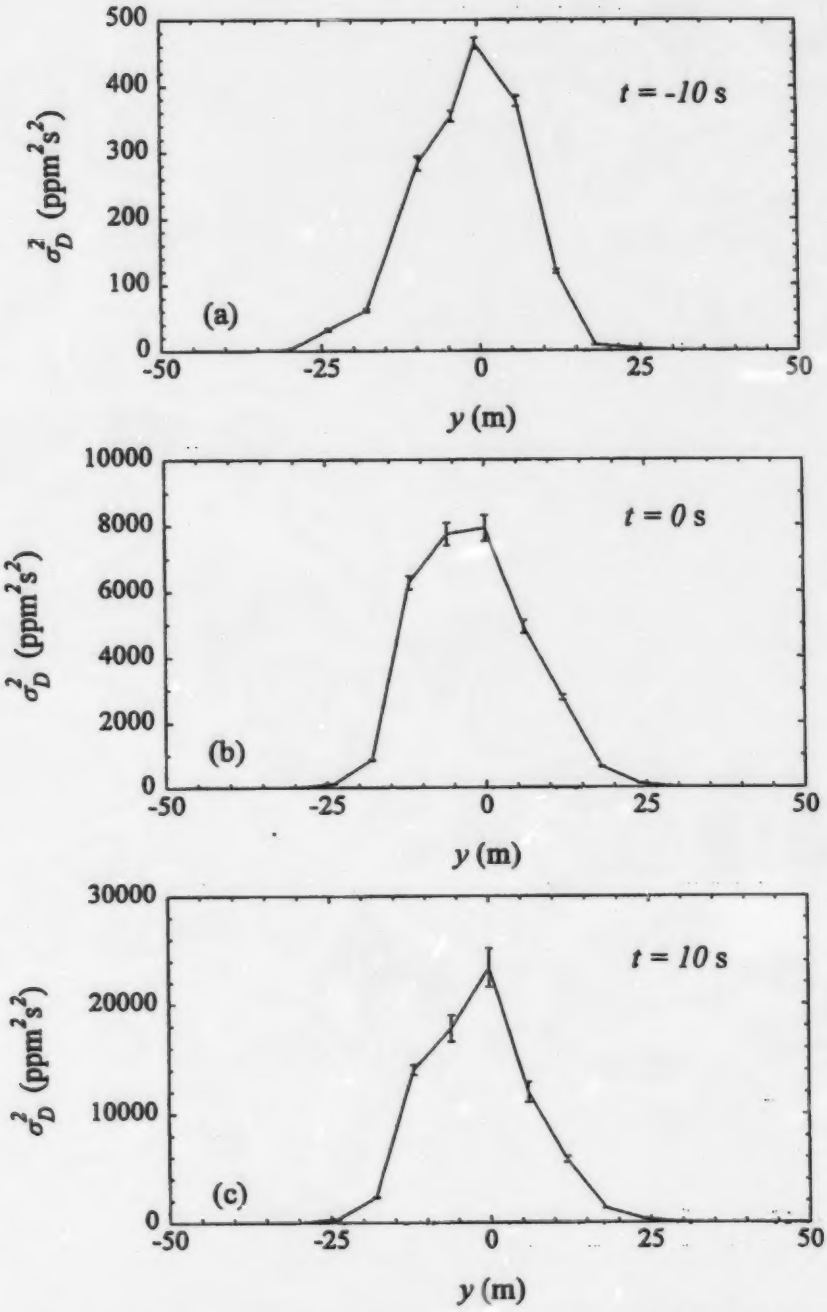

Figure 11. Lateral cross-sections of the dosage variance measured at 3 diffusion times t in the cloud. The data were taken from Ensemble R09. Vertical bars indicate the standard deviation in the estimate for the dosage variance.

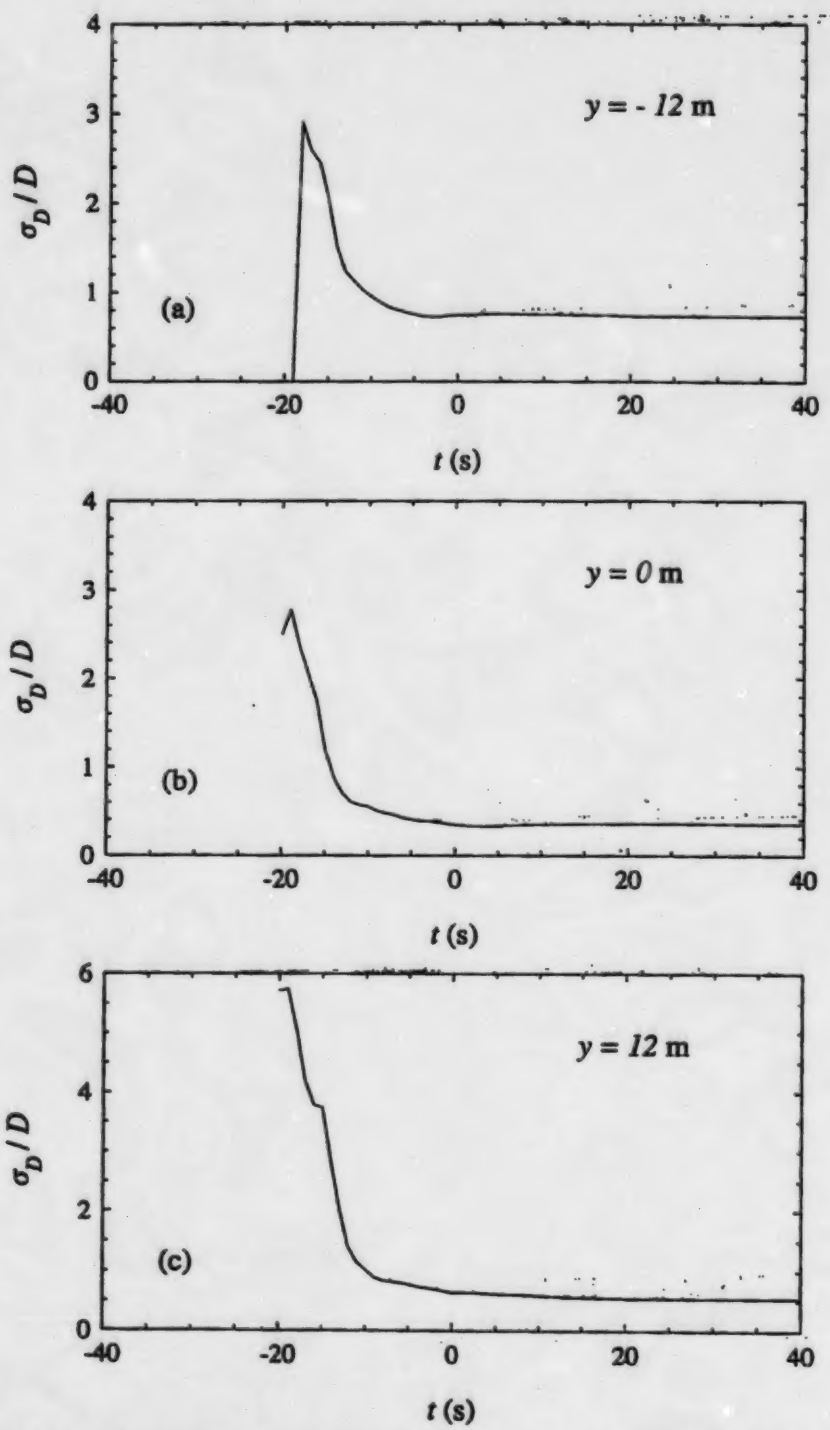

Figure 12. Time profiles of the dosage fluctuation intensity measured at 3 crosswind positions $\overline{y}$ in the cloud. The data were obtained from Ensemble R09.

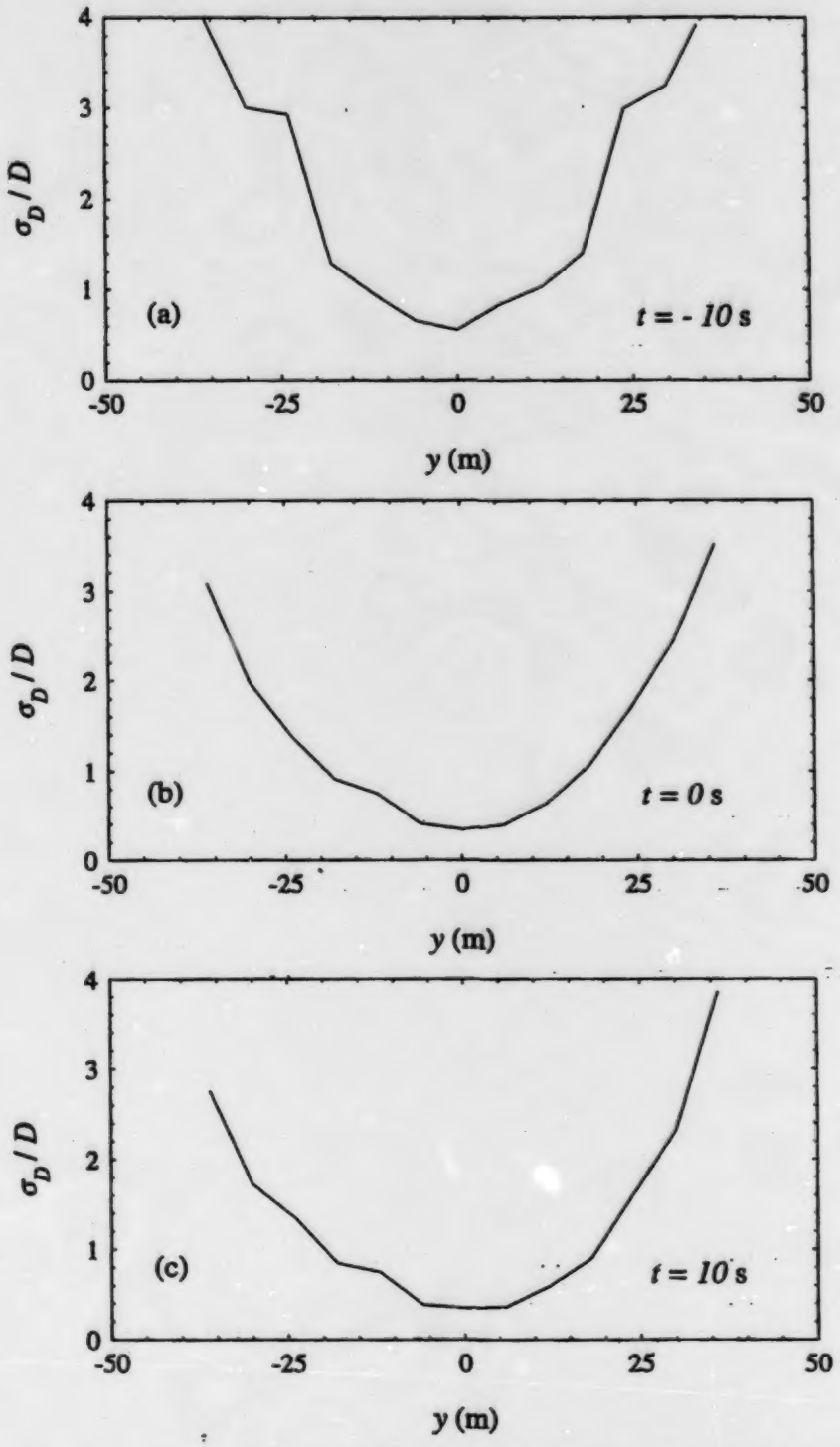

Figure 13. Lateral cross-sections of the dosage fluctuation intensity measured at 3 diffusion times T in the cloud. The data were taken from Ensemble R09.

note that $\sigma_D \approx D$, implying that the dosage fluctuations are not negligible. This is clearly demonstrated in Figures 12 and 13, which show the time profiles and lateral cross-sections of the dosage fluctuation intensity, σ_D/D. Note that the lateral cross-sections of σ_D/D (cf. Figure 13) are qualitatively similar in shape to those of σ_c/C (cf. Figure 7). In particular, crosswind profiles of σ_D/D exhibit an approximate bilateral symmetry about the cloud centroid. However, the intensity of dosage fluctuations at the cloud centre (i.e., at $t = 0$ and $y = 0$) is about 0.3 ± 0.02, which is smaller than the intensity of concentration fluctuations at the cloud centre. The value of the latter quantity is about 0.5 ± 0.01 (cf. Figure 7).

It is noted that the results for the other ensembles are similar to those exhibited for R09. In particular, we will demonstrate next that the scaled crosswind and time profiles of the ensemble-mean concentration and concentration variance exhibit self-similar forms that are independent (approximately or better) of the atmospheric stratification and downwind distance.

4.3. Similarity Forms for Concentration Statistics

Given the ensemble-mean concentration, $C(y, t; x)$, let us define the mean "length" (duration) and "width" of the cloud as follows:

$$\sigma_t(x) \equiv \left\{ \iint t^2 C(y, t; x)\, dt\, dy \Big/ \iint C(y, t; x)\, dt\, dy \right\}^{1/2}, \tag{12a}$$

and

$$\sigma_y(x) \equiv \left\{ \iint y^2 C(y, t; x)\, dt\, dy \Big/ \iint C(y, t; x)\, dt\, dy \right\}^{1/2}. \tag{12b}$$

The explicit dependence of C, σ_t, and σ_y on downwind distance x is indicated in Equation (12); also, recall that it is to be understood implicitly that t and y refer to relative coordinates.

The crosswind profiles of the ensemble-mean concentration C and the concentration variance σ_c^2 at $t = 0$, normalized by the ensemble-mean concentration C_0 and the concentration variance $\sigma_{c,0}^2$ at the centre-of-mass [i.e., the field values evaluated at $(t, y) = (0, 0)$], are plotted against the normalized lateral distance, $y/\sigma_y(x)$, in Figure 14. The subscript 0 is used here, as it will be throughout the paper, to denote the value of any field quantity determined at the cloud centre-of-mass. The data used to construct Figure 14 are taken from the various ensembles whose principal variables are summarized in Table I. Figure 14 shows that the lateral cross-sections of the ensemble-mean concentration and concentration variance have self-preserving forms (i.e., the profiles of C/C_0 and $\sigma_c^2/\sigma_{c,0}^2$ collapse onto the same curves). The solid lines in Figure 14 correspond to Gaussian-type functions of the form

$$\frac{f}{f_0} = \exp\left(-\alpha \left(\frac{y}{\sigma_y}\right)^2\right), \tag{13}$$

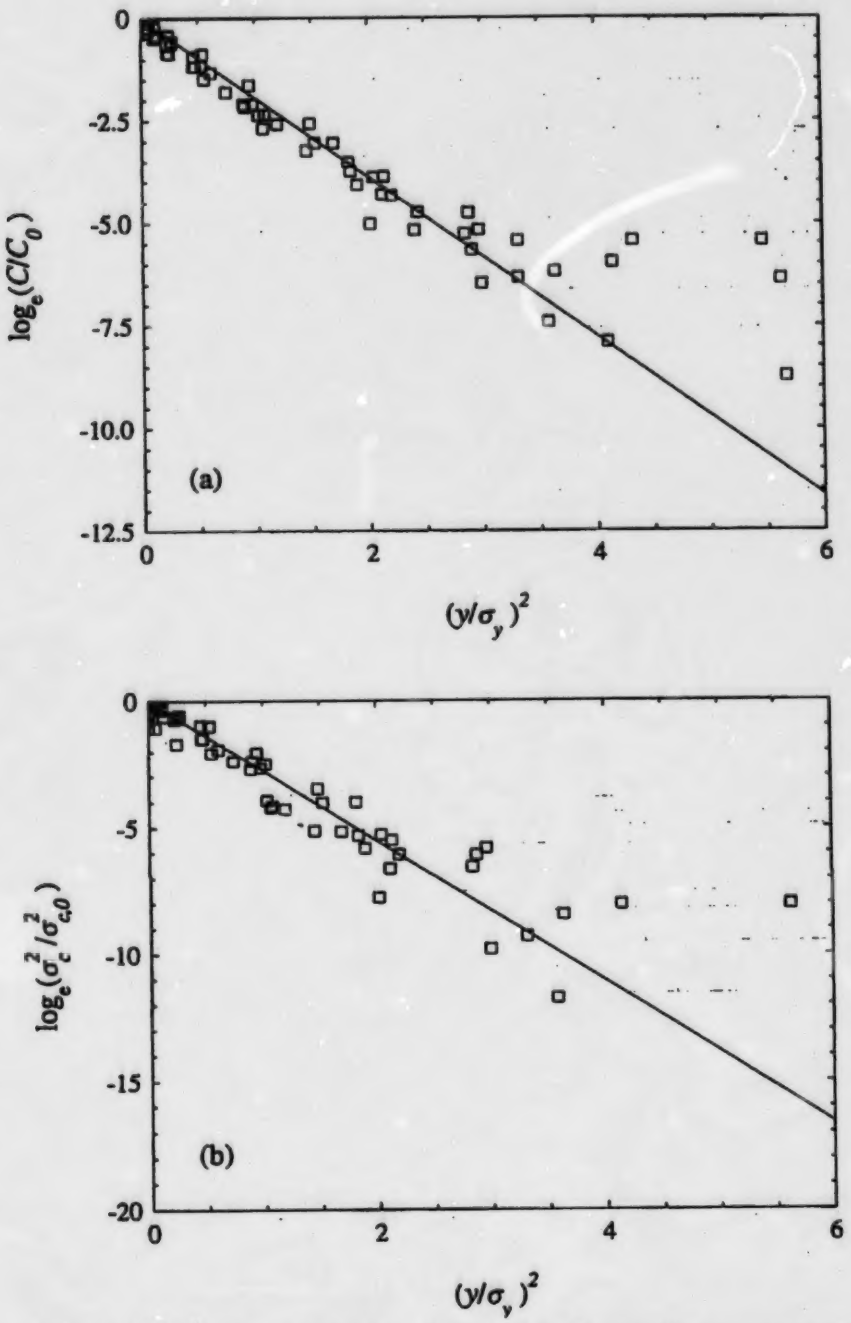

Figure 14. Logarithmic-quadratic plots of (a) normalized ensemble-mean concentration, C/C_0, and (b) normalized concentration variance, $\sigma_c^2/\sigma_{c,0}^2$, at $t = 0$ versus normalized crosswind distance, y/σ_y, for the various ensembles.

because this form is linear on a log-quadratic plot of f versus y/σ_y. The tail slopes, α, for $f \equiv C$ [cf. Figure 14(a)] and $f \equiv \sigma_c^2$ [cf. Figure 14(b)], obtained by least-squares fits for the region $y/\sigma_y \leq 2$, were 1.94 ± 0.03 ($r^2 = 0.99$) and 2.77 ± 0.07 ($r^2 = 0.96$), respectively, where r^2 is the coefficient of determination for the least-squares fit. By virtue of Equation (13), the cloud width c_y defined by Equation (12b) is related to the Gaussian standard deviation, $\sigma_{G,y}$, by

$$\sigma_{G,y} = \frac{\sigma_y}{(2\alpha)^{1/2}}. \tag{14}$$

It must be noted that because the "width" (in the y-direction) and the "length" (in the t-direction) of the ensemble-averaged puff depend on t and y, respectively, and the ensemble-averaged puff concentration is skewed in the t-direction, σ_y obtained using Eq. (12b) does not necessarily have to equal $\sigma_{G,y}$ (i.e., the Gaussian standard deviation for the crosswind ensemble-mean concentration profile at $t = 0$). However, the two quantities are proportional, with the constant of proportionality dependent on the degree of skewness of the ensemble-mean concentration-time profile. In view of the least-squares fitted values of α determined for the crosswind profiles of the ensemble-mean concentration and concentration variance, it is evident that the crosswind Gaussian standard deviation of the mean concentration profile is larger than that of the concentration variance profile by a factor of $\sqrt{2.77/1.94} \approx 1.2$ (viz., the crosswind standard deviation of the mean concentration profile exceeds that of the corresponding concentration variance profile by about 20 percent).

Figure 15 shows a log-quadratic plot of the crosswind profiles of the normalized ensemble-mean dosage D and dosage variance σ_D^2 at $t = 0$ obtained from a number of different ensembles. With the normalizations indicated in Figure 15, it is evident that the crosswind profiles of the ensemble-mean dosage and dosage variance are approximately self-similar. Furthermore, the self-similar forms for D and σ_D^2 are Gaussian [cf. Equation (13)] with $\alpha = 1.74 \pm 0.03$ ($r^2 = 0.98$) and $\alpha = 2.42 \pm 0.06$ ($r^2 = 0.96$), respectively. These fitted values for α are based only on data in the region $y/\sigma_y \leq 2$. As in the case for the concentration, note that the Gaussian crosswind standard deviation of the ensemble-mean dosage profile is larger than that of the dosage variance profile by about 20 percent. It is further noted that the crosswind standard deviations of D and σ_D^2 profiles are slightly larger than those of the corresponding C and σ_C^2 profiles by about 6 percent.

Figures 16(a) and (b) show the normalized ensemble-averaged mean concentration-time profiles at $y = 0$ for $t \leq 0$ (i.e., the rising leading edge of the profiles) and $t \geq 0$ (i.e., the falling trailing edge of the profiles), respectively. Note that time t has been scaled by the mean cloud duration, σ_t, defined by Equation (12a). For the rising leading edge of the profiles, it is evident from the straight line relationships on the log-quadratic plots [cf. Figure 16(a)] that the time profiles of C for $t \leq 0$ are at least as close to Gaussian as the corresponding crosswind

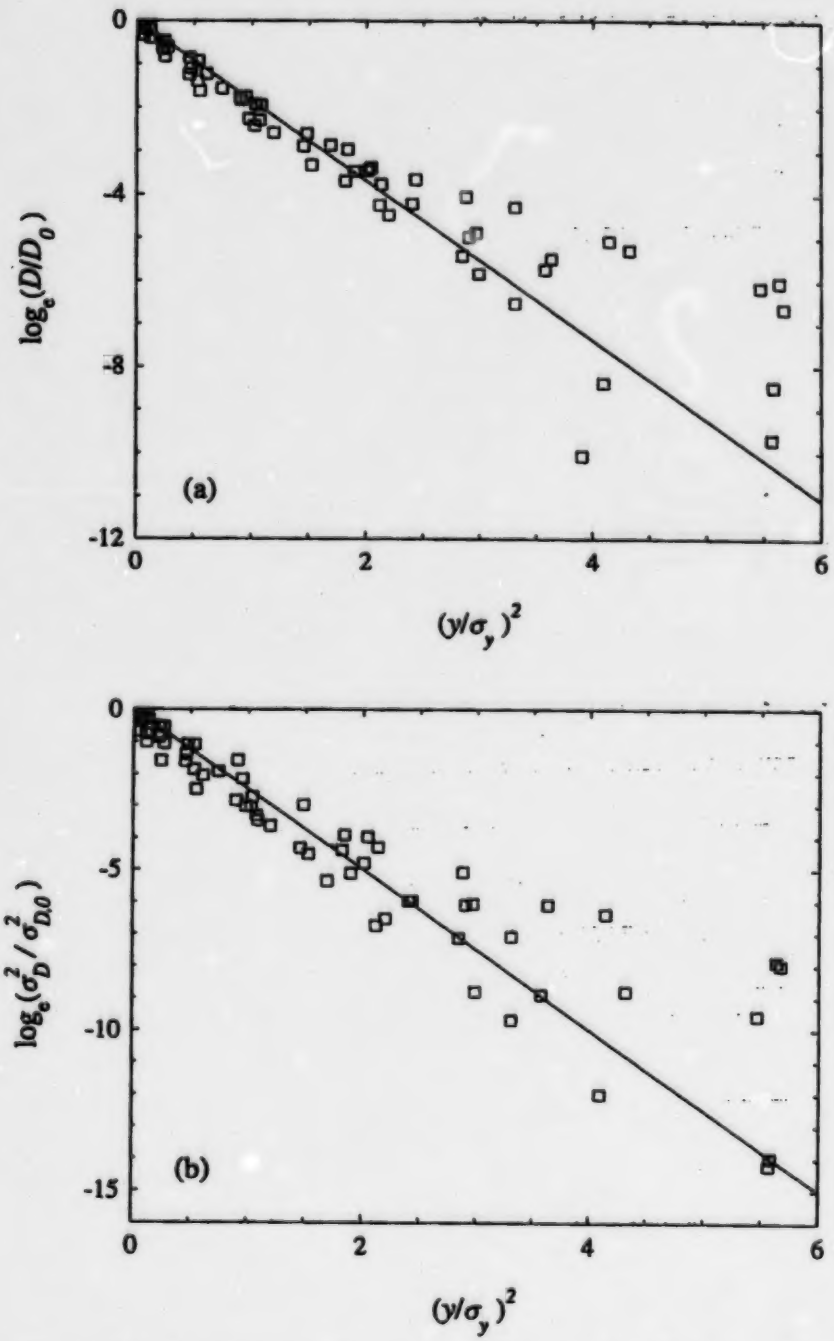

Figure 15. Logarithmic-quadratic plots of (a) normalized ensemble-mean dosage, D/D_0, and (b) normalized dosage variance, $\sigma_D^2/\sigma_{D,0}^2$, at $t = 0$ versus normalized crosswind distance, y/σ_y, for the various ensembles.

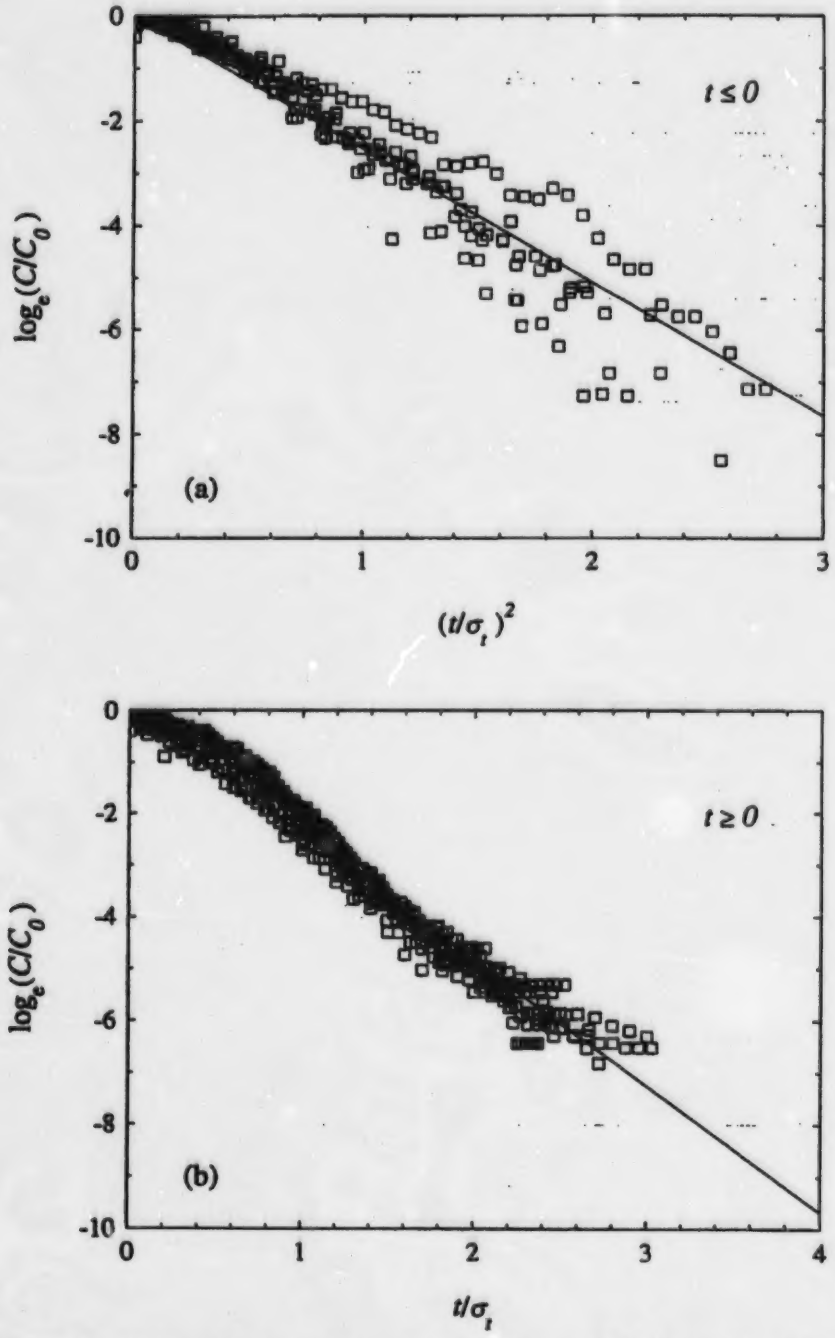

Figure 16. (a) Logarithmic-quadratic plot and (b) logarithmic-linear plot of normalized ensemble-mean concentration, C/C_0, at $y = 0$ versus normalized diffusion time, t/σ_t, for $t \le 0$ and $t \ge 0$, respectively, for the various ensembles.

profiles. For the rising leading edge of the cloud, the mean concentration-time profiles exhibit a general Gaussian similarity form

$$\frac{f}{f_0} = \exp\left(-\beta\left(\frac{t}{\sigma_t}\right)^2\right), \tag{15}$$

with $\beta = 2.56 \pm 0.03$. This regression relation for the leading edge of the mean concentration-time profile explains 96 percent of the observed variation. In contrast to the leading edge of the mean concentration-time profile, which exhibits a Gaussian rise, the trailing edge of the profile appears to show an exponential fall as evidenced from the linearity of the data on the log-linear plot shown in Figure 16(b). Although the log-linear plots of the mean concentration-time profiles for $t \geq 0$ appear to exhibit a quadratic (Gaussian) variation for $t/\sigma_t \lesssim 0.5$, the profiles nevertheless appear to be linear for $t/\sigma_t \gtrsim 0.5$. The trailing edge of the mean concentration-time profiles are approximately self-preserving with the exponential form

$$\frac{f}{f_0} = \exp\left(-\gamma\frac{t}{\sigma_t}\right), \tag{16}$$

with the best fit value of γ of 2.42 ± 0.01 ($r^2 = 0.99$).

Concentration variance time profiles for the leading ($t \leq 0$) and trailing ($t \geq 0$) edges of the cloud at $y = 0$ are exhibited in Figures 17(a) and (b), respectively. It is noted that the time profiles of σ_c^2 are similar in form to those of C, in the sense that both sets of profiles exhibit a rapid self-preserving Gaussian rise in the leading cloud edge and a prolonged self-preserving exponential fall in the trailing cloud edge. However, the best fit values of β and γ [cf. Equations (15) and (16)] for the concentration variance time profiles are 3.39 ± 0.05 ($r^2 = 0.95$) and 4.31 ± 0.03 ($r^2 = 0.98$), respectively. Comparing these values with the corresponding values obtained for the mean concentration-time profiles, it is evident that the time profiles of σ_c^2 rise more rapidly to the peak value in its leading edge and decay more rapidly from the peak value in its trailing edge than the corresponding profiles of C. In particular, the normalized time $t_{1/2}/\sigma_t$ required for the mean concentration-time and concentration variance time profiles to decay to half of their peak values are 0.29 and 0.16, respectively. Here, the normalized half-life is given by $t_{1/2}/\sigma_t = \log_e(2)/\gamma$.

Finally, it is noted that the dosage variance time profiles can be predicted from the form of the concentration variance time profiles, provided the integral time scale, T_c, of concentration fluctuations is known [cf. Equations (9), (10), and (11)]. Figure 18 displays the scaled integral time scale, $T_c/T_{c,0}$, plotted against the normalized time, t/σ_t, at $y = 0$ for data taken from the various ensembles summarized in Table I. The normalized integral time scale curves for the various ensembles

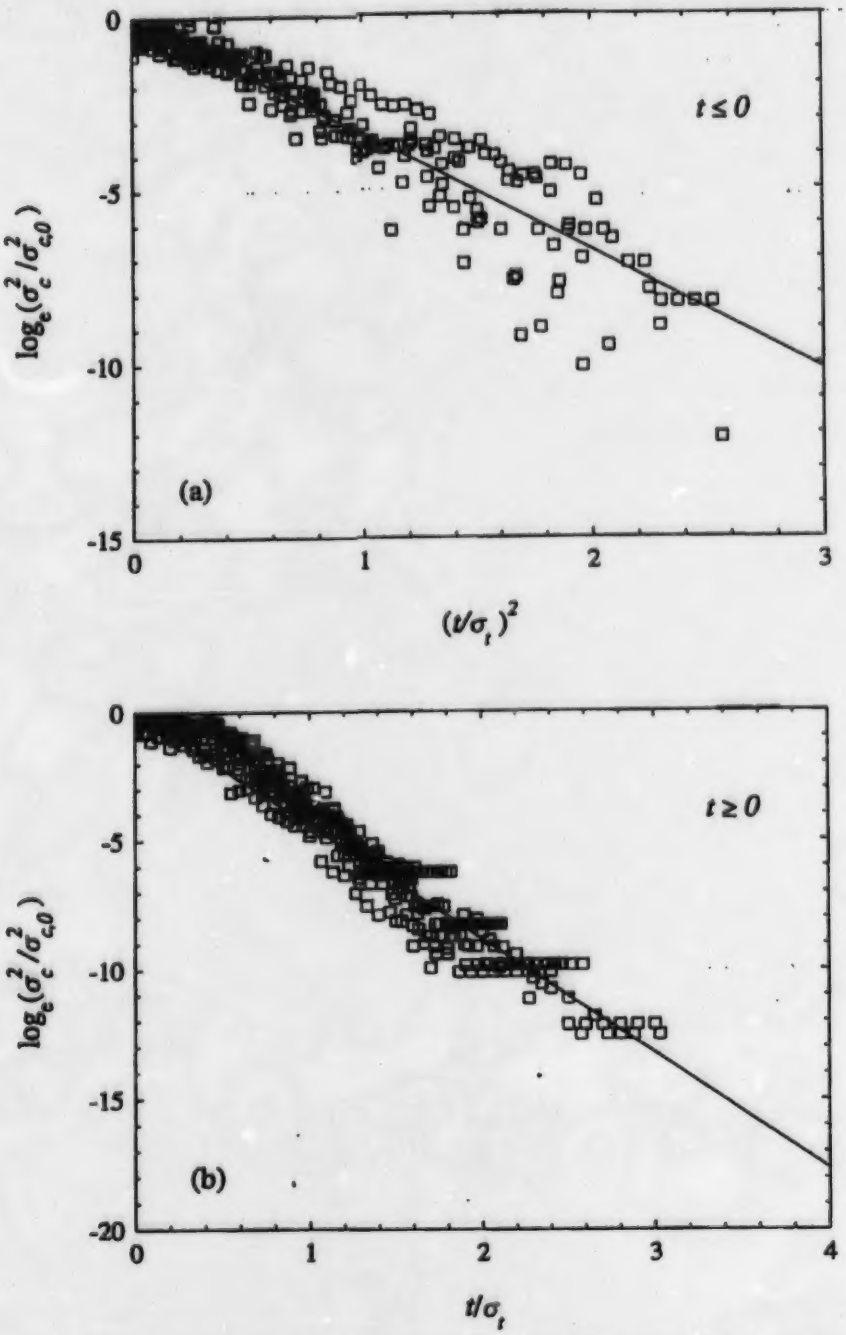

Figure 17. (a) Logarithmic-quadratic plot and (b) logarithmic-linear plot of normalized concentration variance, $\sigma_c^2/\sigma_{c,0}^2$, at $y = 0$ versus normalized diffusion time, t/σ_t, for $t \leq 0$ and $t \geq 0$, respectively, for the various ensembles.

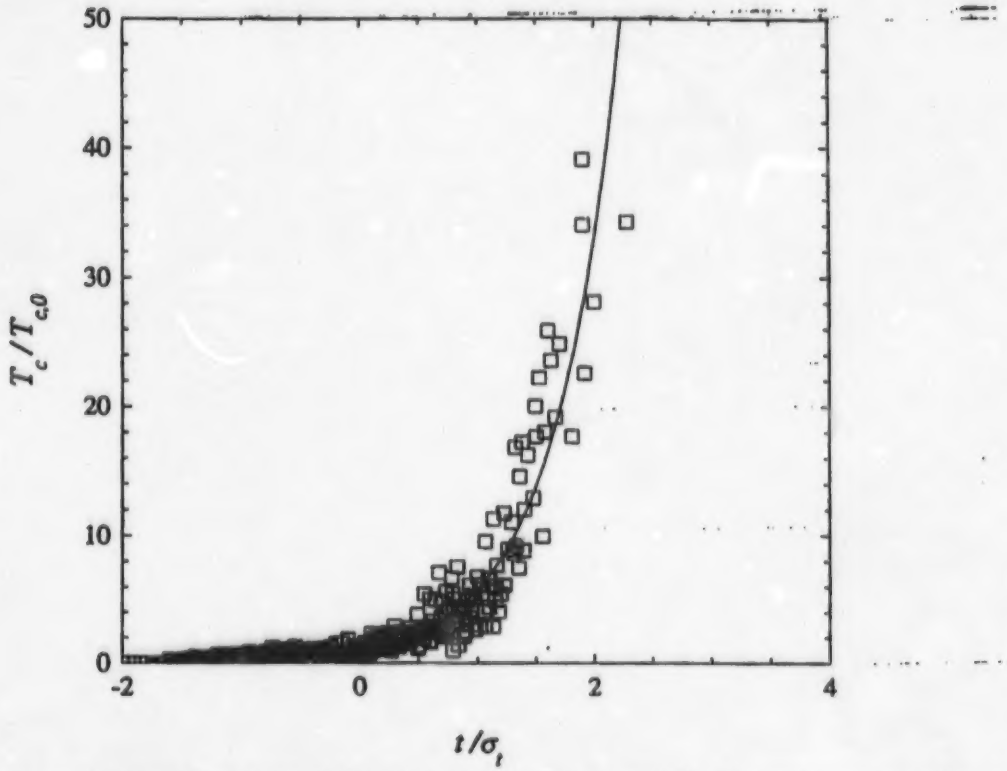

Figure 18. Normalized integral time scale, $T_c/T_{c,0}$, of concentration fluctuations at $y = 0$ as a function of the normalized diffusion time, t/σ_t, for the various ensembles.

collapse well. Interestingly, the general similarity form for the normalized integral time scale appears to be well approximated by an exponential law of the form

$$\frac{T_c}{T_{c,0}} = \exp\left(\frac{7}{4}\frac{t}{\sigma_t}\right), \tag{17}$$

where the constant 7/4 was obtained by a least-squares fit to the data shown in Figure 18. The dependence of T_c on y cannot be determined reliably using the current data. In particular, it must be noted that, due to increasing intermittency in the cloud concentration with increasing $|y|$ (e.g., mixing is likely to entrain clean air at the edges of the instantaneous cloud and, hence, the cloud is more variable with increasing $|y|$), the sample size (i.e., number of realizations in our ensembles) was not sufficient to give a statistically stable estimate of the autocorrelation function [cf. Equation (11)] required to produce an estimate of T_c.

TABLE III

Summary of the mean cloud duration, σ_t, and mean cloud crosswind width, σ_y, used to non-dimensionalize the diffusion time, t, and crosswind distance, y.

Ensemble	σ_t (s)	σ_y (m)
R01	5.0	12.7
R02	5.5	19.4
R03	6.6	12.6
R04	12.2	17.1
R05	11.3	31.1
R06	22.3	52.5
R07	14.0	26.7
R08	15.0	24.3
R09	14.7	17.8
R10	20.3	16.5
R11	15.5	38.5
R12	16.4	55.4
R13	21.8	58.1
R14	30.5	49.3
R15	42.2	29.5
R16	20.2	59.7
R17	36.3	41.1

4.4. Downwind Variation of Cloud Centroid Concentration Statistics

The ensemble-mean concentration and concentration variance crosswind and time profiles and the concentration integral time scale time profile, when normalized by their corresponding cloud centroid values, were found to assume approximately self-preserving forms when these profiles were plotted against either a scaled crosswind distance or a scaled time. In this section, we focus on the downwind variation of the various quantities used to non-dimensionalize either the concentration statistics or the crosswind distance and (diffusion) time. For reference, the values of these quantities are given in Tables III and IV.

Because the diffusion experiments reported here involved near ground-source instantaneous releases over relatively short downwind fetches (e.g., $x \lesssim 1200$

TABLE IV

Summary of the cloud centroid values used to non-dimensionalize the various crosswind and time profiles of concentration amplitude and temporal statistics. Here, C_0 is the value of the ensemble-mean concentration at the cloud centroid; $\sigma^2_{c,0}$ is the value of the concentration variance at the cloud centroid; D_0 is the value of the ensemble-mean dosage at the cloud centroid; $\sigma^2_{D,0}$ is the value of the dosage variance at the cloud centroid; and, $T_{c,0}$ is the value of the integral time scale of concentration fluctuations at the cloud centroid.

Ensemble	C_0 (ppm)	$\sigma^2_{c,0}$ (ppm^2)	D_0 (ppm s)	$\sigma^2_{D,0}$ (ppm^2 s^2)	$T_{c,0}$ (s)
R01	33.02	1245	155.3	9489	1.07
R02	37.83	1434	178.2	8505	0.88
R03	62.90	1805	301.6	16230	1.30
R04	3.16	10.02	37.88	685.5	2.63
R05	0.77	1.22	6.71	51.42	2.56
R06	1.99	11.42	19.36	297.4	2.17
R07	4.56	80.89	45.86	5676	2.56
R08	12.74	112.4	144.6	12080	4.24
R09	26.95	129.3	260.3	7916	4.00
R10	18.68	82.03	386.0	10650	5.13
R11	2.29	5.46	23.24	428.4	3.73
R12	3.62	5.08	39.43	311.6	3.27
R13	1.75	1.88	26.10	484.2	5.36
R14	4.21	11.59	86.84	4341	17.71
R15	11.66	30.80	344.4	17190	15.38
R16	1.58	1.37	21.62	352.0	8.77
R17	5.70	4.41	129.9	1588	17.46

m), implying that the diffusion occurred mainly in the atmospheric surface layer, it is useful to apply the surface-layer "similarity theory" of Monin and Obukhov (1954) in order to try to order the behaviour of the mean cloud sizes and cloud centroid concentration statistics. Applying the surface-layer similarity of Monin and Obukhov in the present context, it is hypothesized that the various quantities used to normalize diffusion time and the various concentration amplitude and temporal statistics summarized in Tables III and IV can be ordered provided they are non-dimensionalized by appropriate combinations of the key (primary) variables that determine the characteristics of the surface layer and the source release; namely, u_*, the surface friction velocity that is indicative of the shear stress at the ground; L, the Obukhov length, which can be regarded as a stability parameter and itself is

defined by the surface fluxes of heat and momentum; and Q, the source strength (release mass). For any quantity, Ψ, describing the dispersing cloud and which varies with downwind distance (e.g., mean cloud width and duration, ensemble-mean concentration and dosage, concentration and dosage variance), application of dimensional analysis with the primary variables enumerated above leads to consideration of the relationship

$$\Psi = \Psi_* \mathcal{F}\left(\frac{x}{|L|}\right),$$

where Ψ_* is a combination of the primary variables that has the same dimensions as Ψ. Here, $\mathcal{F}(\cdot)$ is a similarity function that relates the dimensionless variable Ψ/Ψ_* and $x/|L|$; its precise form must be determined from experimental data. Surface-layer similarity has been applied extensively to investigate the downwind variation of plume width growth rates and cross-wind integrated mean (time-averaged) plume concentrations resulting from continuously emitting sources in the atmospheric surface layer (Briggs, 1982; Venkatram, 1992; Venkatram and Du, 1997).

Using the surface-layer similarity, the mean puff crosswind width σ_y [cf. Equation (12b)] scales as $\sigma_y/|L|$ and the mean puff "duration" [cf. Equation (12a)] as $\sigma_t u_*/|L|$ to yield the properly normalized quantities. Figures 19(a) and (b) exhibit the downwind evolution of the non-dimensionalized mean crosswind puff width and "duration", respectively. It is seen that both non-dimensional crosswind puff width and duration display a nearly linear growth (i.e., proportional to $\left(x/|L|\right)^{1.17}$ and $\left(x/|L|\right)^{0.96}$, respectively), indicating the cloud is in the turbulent-convective regime of development over the range of atmospheric conditions and downwind distances covered by our results. It must be noted that because of the limited range in σ_y, $u_*\sigma_t$, and x compared to $|L|$, a portion of the linear growth observed in Figure 19 may result simply from the variation in $|L|$ and the scaling adopted here. This issue is difficult to assess, other than to indicate that plots of σ_y and $u_*\sigma_t$ versus x (excluding those ensembles corresponding to the most unstable atmospheric conditions at each downwind distance) also appear to show an approximate linear dependence with x, albeit with more scatter in the data points than exhibited in Figures 19(a) and (b) (i.e., the variation of these quantities now depends on both the turbulence characteristics and x).

Next, we seek a relationship between the normalized ensemble-mean concentration at the cloud centroid, $C_0|L|^3/Q$, and the normalized downwind distance, $x/|L|$, which are plotted in Figure 20(a). From Figure 20(a), we see that $C_0|L|^3/Q$ is approximately proportional to $\left(x/|L|\right)^{-3.6}$, with a coefficient of determination r^2 of 0.97. In greater detail, the downwind variation of C_0 can be adequately expressed by the relationship

$$\frac{C_0|L|^3}{Q} = 6600\left(\frac{x}{|L|}\right)^{-3.6}. \tag{18}$$

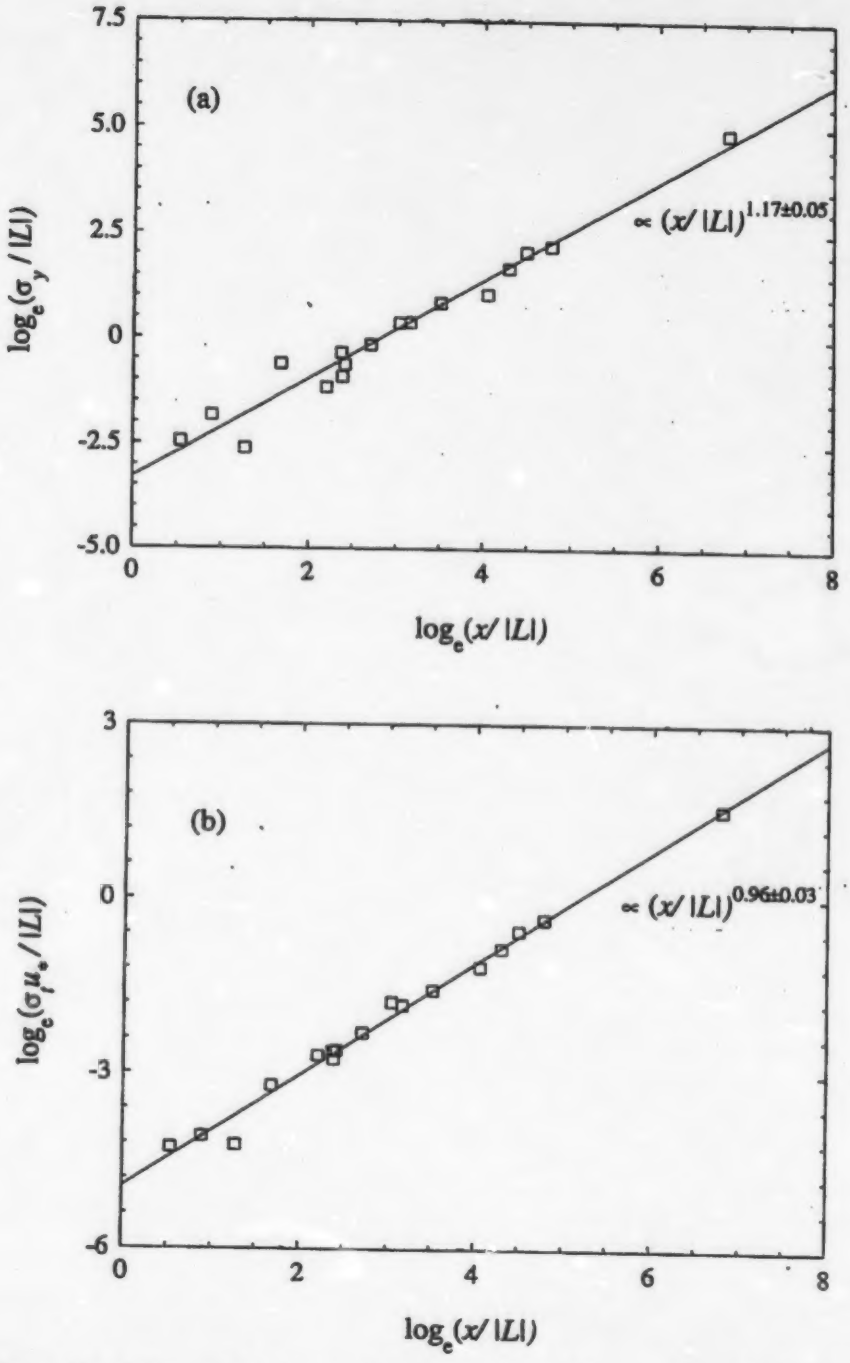

Figure 19. (a) Normalized crosswind cloud width, $\sigma_y/|L|$, at $t = 0$, and (b) normalized cloud duration, $\sigma_t u_*/|L|$, at $y = 0$ plotted against normalized downwind distance, $x/|L|$, on a log-log scale for the various ensembles.

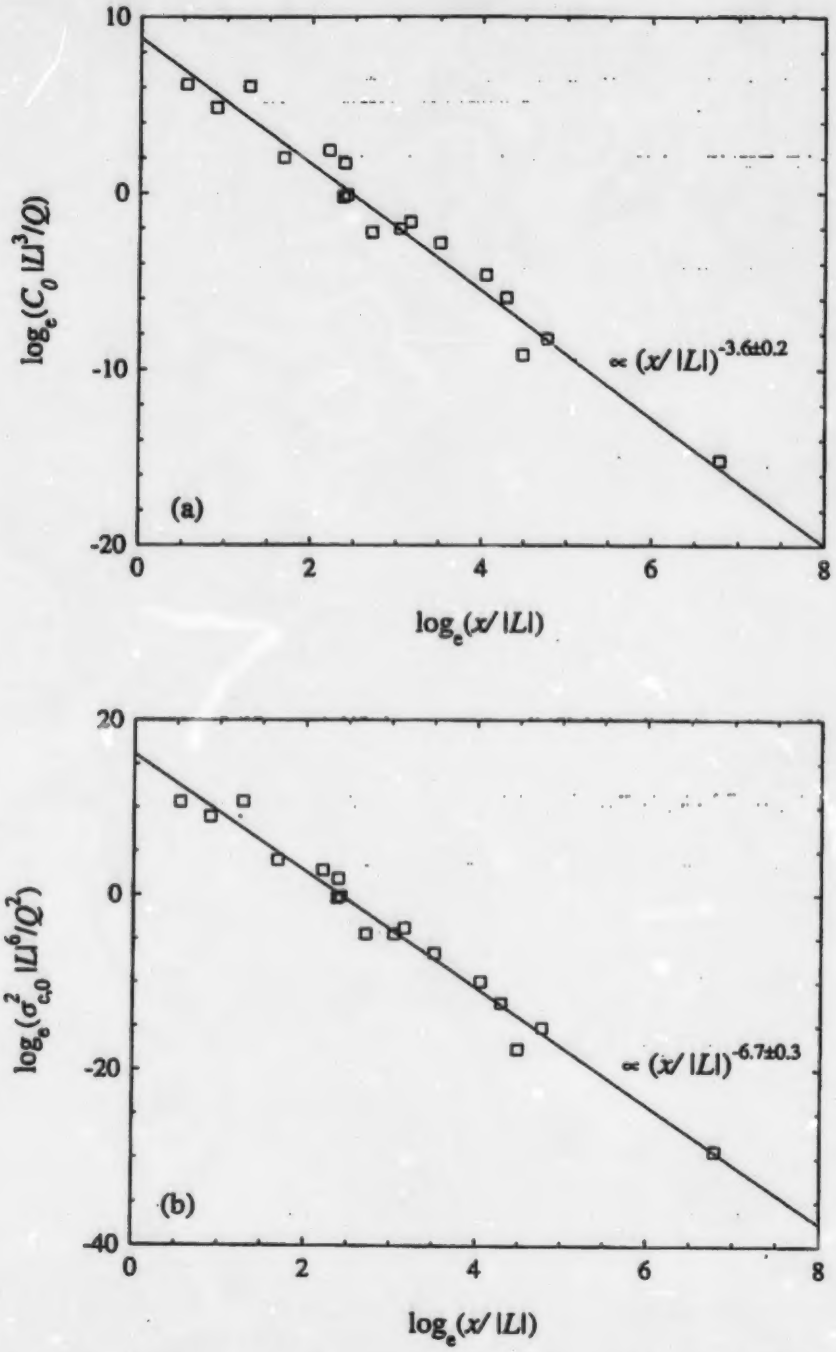

Figure 20. (a) Normalized ensemble-mean concentration, $C_0|L|^3/Q$, and (b) normalized concentration variance, $\sigma^2_{c,0}|L|^6/Q^2$, at the cloud centre plotted against normalized downwind distance, $x/|L|$, on a log-log scale for the various ensembles.

Interestingly, $C_0|L|^3/Q \propto (x/|L|)^{-3.6}$ appears to be valid no matter what the atmospheric stratification for quite an extended range of travel distances (e.g., $x/|L| \lesssim 1000$). This contrasts markedly with the downwind variation of the normalized cross-wind integrated concentration, $C_*^y \equiv C^y u_*|L|/Q_c$ (Q_c is the source emission rate), where it has been found that C_*^y is independent of atmospheric stability only for short travel distances $x/|L| \lesssim 2$ where C_*^y varies as $(x/|L|)^{-1}$ (Venkatram and Du, 1997).

Similarly, Figure 20(b) displays the dimensionless concentration variance at the cloud centroid, $\sigma_{c,0}^2|L|^6/Q^2$, as a function of $x/|L|$. Note that over the range of conditions and downwind distances covered by our field experiments, the normalized $\sigma_{c,0}^2$ appears to be independent of the stratification stability and varies like $(x/|L|)^{-6.7}$. In particular, the downwind evolution of $\sigma_{c,0}^2$ is well characterised by

$$\frac{\sigma_{c,0}^2|L|^6}{Q^2} = 9350\left(\frac{x}{|L|}\right)^{-6.7}. \tag{19}$$

Note that the power-law exponent for the downwind decay of $\sigma_{c,0}^2$ is roughly twice that of C_0. Hence, it is seen that the concentration standard deviation $\sigma_{c,0}$ falls off with downwind distance roughly as fast as the mean concentration C_0. Indeed, from Equations (18) and (19) it can be deduced that the relative intensity of concentration fluctuations, $\sigma_{c,0}/C_0$, at the cloud centroid varies as $(x/|L|)^s$, where $s = 0.25 \pm 0.2$ (s.d.). Hence, the relative concentration fluctuation intensity is seen to change very slowly with downwind distance.

Figures 21(a) and (b) show plots of the normalized ensemble-mean dosage and dosage variance at the cloud centre, respectively, versus the normalized downwind distance. Again, the consistency of the normalized data is good, and the scatter is small enough to specify with accuracy a single "universal" exponent in the power-law representation of the variation of normalized D_0 and $\sigma_{D,0}^2$ with downwind distance. In particular, the points for normalized D_0 and $\sigma_{D,0}^2$ lie close to the power-law relationships

$$\frac{D_0 u_*|L|^2}{Q} = 43\left(\frac{x}{|L|}\right)^{-2.7}, \tag{20}$$

and

$$\frac{\sigma_{D,0}^2 u_*^2|L|^4}{Q^2} = 180\left(\frac{x}{|L|}\right)^{-4.9}, \tag{21}$$

respectively. The coefficients of determination for these two least-squares fits are both 0.95. Note that the rates of decrease of normalized D_0 and $\sigma_{D,0}^2$ with non-dimensional distance $x/|L|$ are slower than those for normalized C_0 and $\sigma_{c,0}^2$. Indeed, Equations (18) and (20) seem to suggest that, if the rates of downwind

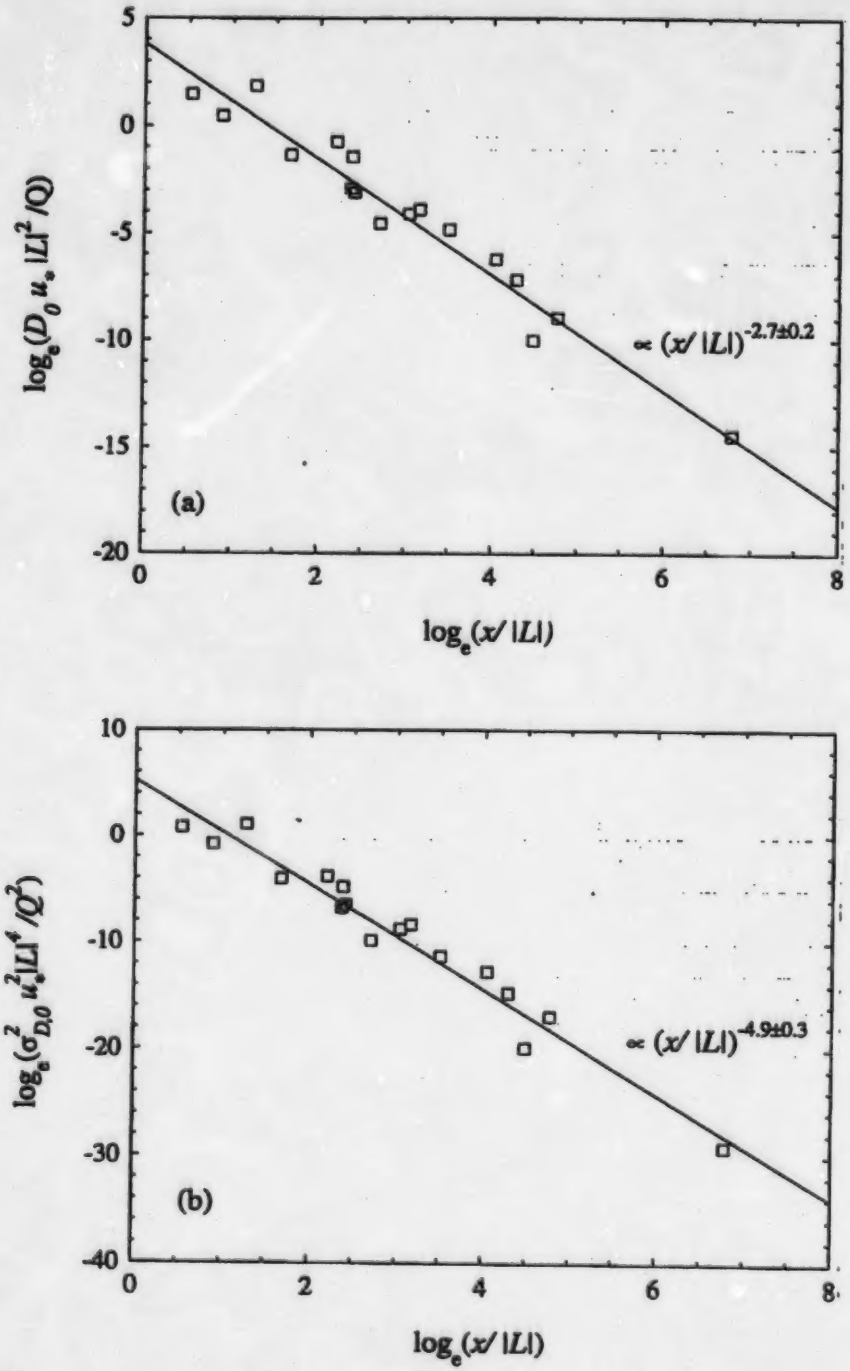

Figure 21. (a) Normalized ensemble-mean dosage, $D_0 u_* |L|^2/Q$, and (b) normalized dosage variance, $\sigma^2_{D,0} u_*^2 |L|^4/Q^2$, at the cloud centre plotted against normalized downwind distance, $x/|L|$, on a log-log scale for the various ensembles.

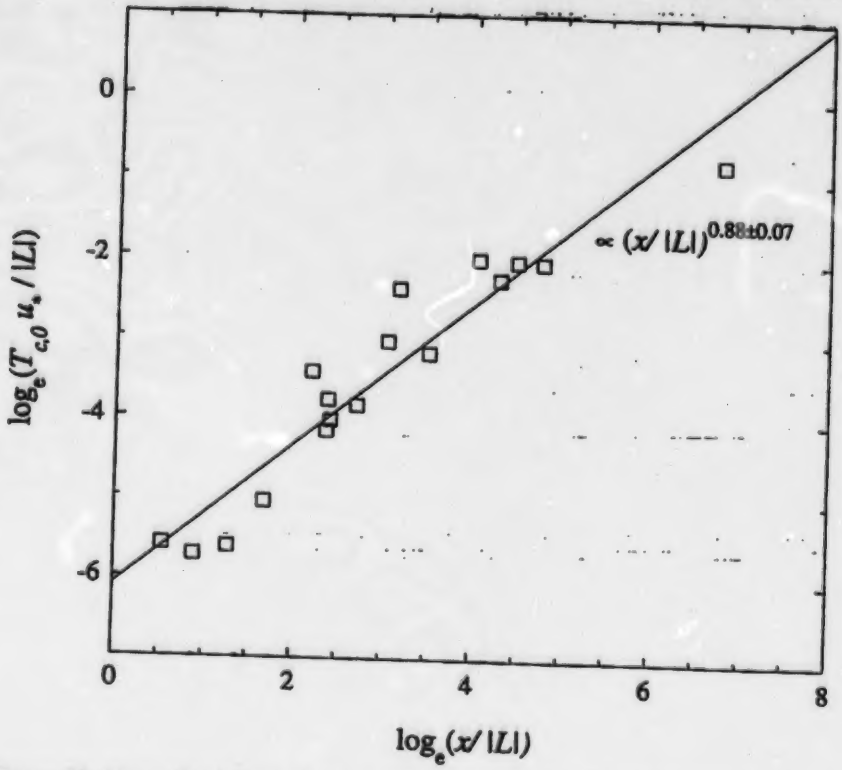

Figure 22. Normalized integral time scale, $T_{c,0}u_*/|L|$, of concentration fluctuations at the cloud centre plotted against normalized downwind distance, $x/|L|$, on a log-log scale for the various ensembles.

decay in normalized C_0 and D_0 are proportional to $(x/|L|)^p$ and $(x/|L|)^r$, respectively, then the exponents p and r are related as $r = p+1$. It must be noted that this difference between p and r in the downwind decays of C_0 and D_0 is consistent with a Gaussian puff model of the cloud concentration (Csanady, 1973), which relates the difference between them to the power-law exponent for the downwind growth of σ_r [which, in our case, is 0.96 from Fig. 19(b)]. Similarly, Equations (19) and (21) seem to indicate that, if p and r are the power-law exponents in the power-law functions characterizing the downwind decay of normalized $\sigma^2_{c,0}$ and $\sigma^2_{D,0}$, respectively, then these exponents are related (approximately or better) by $r = p + 2$. Finally, Equations (20) and (21) imply that the relative dosage fluctuation intensity at the cloud centre varies with downwind distance as $(x/|L|)^s$, with $s = 0.35 \pm 0.2$ (s.d.). Hence, the downwind variation of the fluctuation intensities of concentration and dosage at the cloud centre are roughly equal, and both appear to vary slowly with downwind distance.

The downwind development of the normalized integral time scale of concentration fluctuations at the cloud centre is presented in Figure 22. Although there is more scatter in the measured $T_{c,0}$ values, the normalized integral time scale

$T_{c,0}u_*/|L|$ is seen to increase approximately proportionally to $x/|L|$ over the range of atmospheric conditions and downwind distances encompassed by our experiments. A least-squares line of best fit to the data suggests the following power-law relationship for the downwind variation of the integral time scale:

$$\frac{T_{c,0}u_*}{|L|} = 0.0022\left(\frac{x}{|L|}\right)^{0.88}, \tag{22}$$

with a coefficient of variation $r^2 = 0.91$. Interestingly, the integral time scale of concentration fluctuations $T_{c,0}$ increases roughly proportionally to either σ_y or σ_t. Furthermore, it is noted that $T_{c,0}$ is comparable in magnitude to σ_t (as well as exhibiting a similar decay law with downwind distance) suggesting that most of the concentration variability (energy) occurs at the scale of the puff "size".

5. Summary and Conclusions

An extensive new dataset of instantaneous concentration measurements in clouds, which includes simultaneous meteorological and turbulence measurements, has been analyzed to provide a wealth of new information on the dispersion of contaminant clouds in the atmospheric surface layer. Experiments were conducted over a wide range of atmospheric conditions (from very unstable to moderately stable conditions) with downwind fetches of between 200 m and 1200 m. The unique feature of these experiments was the performance of a sufficient number of controlled repeat releases to enable the behaviour of concentration fluctuations in the dispersing cloud to be studied. This is important because the measurement of concentration fluctuations in clouds dispersing in the atmosphere, in contrast to plumes, is virtually non-existent. As a result of the current series of tracer dispersion experiments, a fairly detailed picture of the crosswind and temporal structure of concentration fluctuation statistics in a dispersing cloud for relative turbulent diffusion has been obtained.

A number of statistical properties of concentration fluctuations in clouds has been extracted. These include the mean cloud crosswind width and mean cloud duration (persistency); crosswind and time profiles of ensemble-mean concentration, concentration variance, ensemble-mean dosage and dosage variance; and, time profiles of the integral time scale of concentration fluctuations. Generally, the fluctuation statistics measured in dispersing clouds are qualitatively similar to those observed in dispersing plumes (cf., Dinar et al., 1988; Mylne and Mason, 1991; Yee et al., 1994a, among others). Ensemble-mean concentration-time profiles are positively skewed. However, crosswind profiles of ensemble-mean concentration and dosage are Gaussian (approximately or better). The shapes of the time and crosswind profiles of concentration variance and dosage variance are qualitatively similar to those of the corresponding mean concentration and dosage, respectively,

although there are some quantitative differences. It is demonstrated that even in the framework of relative diffusion, the fluctuation intensities of concentration and dosage vary strongly in the crosswind direction. Indeed, crosswind profiles of concentration and dosage fluctuation intensities have a minimum at the cloud centre and increase toward the cloud fringes and, in this sense, resemble qualitatively lateral cross-sections of σ_c/C measured in plumes (Mylne and Mason, 1991; Yee et al., 1994a). However, unlike plumes where the lateral variation of fluctuation intensity is due primarily to meander, the variation in clouds in the relative diffusion framework is attributable to internal stirring and mixing processes only.

The downwind evolution of various cloud concentration statistics at the centroid has been studied using surface-layer similarity scaling. It is shown that this scaling provides a systematic ordering to all the data. Furthermore, the scaling yields some approximate universal relationships for the relative diffusion of clouds in the surface layer. Present new measurements of the non-dimensional cloud centre ensemble-mean concentration ($C_0^* \equiv C_0|L|^3/Q$) and dosage ($D_0^* \equiv D_0 u_*|L|^2/Q$) in relative diffusion show that the behaviour of these two quantities is well approximated by the power-law relationships, $C_0^* \propto (x/|L|)^{-p}$ and $D_0^* \propto (x/|L|)^{-p+1}$ with $p \approx 3.6$. Furthermore, the data support the following descriptions for the downwind variation of the cloud centre concentration variance ($\sigma_{c,0}^{2*} \equiv \sigma_{c,0}^2|L|^6/Q^2$) and dosage variance ($\sigma_{D,0}^{2*} \equiv \sigma_{D,0}^2 u_*^2|L|^4/Q^2$): $\sigma_{c,0}^{2*} \propto (x/|L|)^{-p}$ and $\sigma_{D,0}^{2*} \propto (x/|L|)^{-p+2}$, where $p \approx 6.7$. Finally, for the range of atmospheric conditions and downwind fetches covered by the data, the mean cloud crosswind width, σ_y, the mean cloud duration, σ_t, and the cloud centre integral time scale of concentration fluctuations, $T_{c,0}$, were found to increase linearly (approximately or better) with non-dimensional distance, $x/|L|$.

These relationships imply that cloud centroid fluctuation intensities of concentration, $\sigma_{c,0}/C_0$, and dosage, $\sigma_{D,0}/D_0$, are very weak functions of downwind distance (or, equivalently, cloud travel time) since it is seen that the concentration and dosage standard deviations, $\sigma_{c,0}$ and $\sigma_{D,0}$, fall off with x roughly as fast, respectively, as the mean concentration and dosage, C_0 and D_0. In particular, it is seen that $\sigma_{c,0}/C_0$ and $\sigma_{D,0}/D_0$ vary like $(x/|L|)^s$ where $s \approx 0.3 \pm 0.2$ (s.d.). Hence, the fluctuation intensities of concentration and dosage appear to increase like $x^{0.3}$ in the turbulent convective regime of cloud development, wherein the cloud size increases linearly with downwind distance (or, equivalently, travel time). However, it must be stressed that this putative rate of increase in the centroid fluctuation intensities of concentration and dosage is very small. Indeed, the alternative interpretation that these fluctuation intensities achieve near-constancy in level with downwind distance within the turbulent-convective regime of cloud development cannot be ruled out, given the experimental scatter in our data.

Crosswind profiles of the ensemble-mean concentration and dosage, when normalized by their values at the cloud centre, assume self-similar Gaussian forms. However, it was found that the crosswind standard deviation of the ensemble-mean

dosage profile was larger than that of the ensemble-mean concentration profile by roughly 6 percent. Furthermore, the concentration variance and dosage variance crosswind profiles, when normalized by their cloud centre values, collapse to a self-preserving Gaussian form, but with crosswind standard deviations that are only about 80 percent those of the corresponding ensemble-mean concentration and dosage profiles, respectively. Ensemble-mean concentration-time and concentration variance time profiles, when scaled by their cloud centre values, exhibit an asymmetrical self-similar form: viz., there is a rapid self-preserving Gaussian rise in the leading (front) part of the cloud up to the cloud centre, followed by an elongated self-preserving exponential fall in the trailing (back) part of the cloud. It was found that the normalized concentration variance time profile exhibits a faster rise to, and a subsequent faster descent from, its peak value than the ensemble-mean concentration-time profiles. In particular, the non-dimensional half-life, $t^*_{1/2} \equiv t_{1/2}/\sigma_t$, (i.e., the time taken for a normalized quantity to fall to one-half of its peak value) of the ensemble-mean concentration is roughly twice that of the corresponding concentration variance (e.g., $t^*_{1/2}$ is roughly 0.3 for the mean concentration, whereas it is approximately 0.15 for the concentration variance). Finally, the time profiles of the integral time scale of concentration fluctuations, when non-dimensionalized by their cloud centre values, were found to possess the self-similar exponential form $\exp(\frac{7}{4}t/\sigma_t)$.

Acknowledgements

This work was supported partially by Defence Special Weapons Agency.

References

Box, G. E. P. and Tiao, G. C.: 1992, *Bayesian Inference in Statistical Analysis*, Wiley, New York, 588 pp.

Briggs, G. A.: 1982, 'Similarity Forms for Ground-Source Surface-Layer Diffusion', *Boundary-Layer Meteorol.* 23, 489–502.

Csanady, G. T.: 1973, *Turbulent Diffusion in the Environment*, D. Reidel Publishing Company, Dordrecht, Holland, 280 pp.

Dinar, N., Kaplan, H., and Kleiman, M.: 1988, 'Characterization of Concentration Fluctuations of a Surface Plume in a Neutral Boundary Layer', *Boundary-Layer Meteorol.* 45, 157–175.

Hall, D. J., Walters, R. A., Marsland, G. W., Upton, S. L., and Emmott, M. A.: 1991, 'Repeat Variability in Instantaneously Released Heavy Gas Clouds – Some Wind Tunnel Experiments', Technical Report LR 804(PA), Warren Spring Laboratory, Stevenage, England, 74 pp.

Hanna, S. R.: 1984, 'The Exponential Probability Density Function and Concentration Fluctuations in Smoke Plumes', *Boundary-Layer Meteorol.* 29, 361–375.

Kendall, M. and Stuart, A.: 1977, *The Advanced Theory of Statistics*, Charles Griffin, London, 455 pp.

Meroney, R. N. and Lohmeyer, A.: 1984, 'Statistical Characteristics of Instantaneous Dense Gas Clouds Released in an Atmospheric Boundary-Layer Wind Tunnel', *Boundary-Layer Meteorol.* **28**, 1–22.

Monin, A. S. and Obukhov, A. M.: 1954: 'Basic Laws of Turbulent Mixing in the Atmosphere Near the Ground', *Tr. Akad. Nauk. SSSR Geofiz. Inst.*, No. 24 (151), 163–187.

Mylne, K. R.: 1993, 'The Vertical Profile of Concentration Fluctuations in Near-Surface Plumes', *Boundary-Layer Meteorol.* **65**, 111–136.

Mylne, K. R. and Mason, P. J.: 1991, 'Concentration Fluctuation Measurements in a Dispersing Plume at a Range of up to 1000 m', *Quart. J. Roy. Meteorol. Soc.* **117**, 177–206.

Parzen, E.: 1960, *Modern Probability Theory and Its Applications*, John Wiley & Sons, Inc., New York, 464 pp.

Peterson, H., Lamb, B., and Stock, D.: 1990, 'Interpretation of Measured Tracer Concentration Fluctuations Using a Sinsusoid Meandering Plume Model', *J. Appl. Meteorol.* **29**, 1284–1299.

Sawford, B. L., Frost, C. C., and Allan, T. C.: 1985, 'Atmospheric Boundary-Layer Measurements of Concentration Statistics from Isolated and Multiple Sources', *Boundary-Layer Meteorol.* **31**, 249–268.

Sweatman, W. L. and Chatwin, P. C.: 1996, 'Dosages From Instantaneous Releases of Dense Gases in Wind Tunnels and Into a Neutrally Stable Atmosphere', *Boundary-Layer Meteorol.* **77**, 211–231.

Venkatram, A.: 1992, 'Vertical Dispersion of Ground-Level Releases in the Surface Boundary Layer', *Atmos. Environ.* **26A**, 947–949.

Venkatram, A. and Du, S.: 1997, 'An Analysis of the Asymptotic Behavior of Cross-Wind Integrated Ground-Level Concentrations Using Lagrangian Stochastic Simulation', *Atmos. Environ.* **31**, 1467–1476.

Yee, E., Chan, R., Kosteniuk, P. R., Chandler, G. M., Biltoft, C. A., and Bowers, J. F.: 1994a, 'Experimental Measurements of Concentration Fluctuations and Scales in a Dispersing Plume in the Atmospheric Surface Layer Obtained Using a Very Fast-Response Concentration Detector', *J. Appl. Meteorol.* **33**, 996–1016.

Yee, E., Chan, R., Kosteniuk, P. R., Chandler, G. M., Biltoft, C. A., and Bowers, J. F.: 1994b, 'Concentration Fluctuation Measurements in Clouds Released From a Quasi-Instantaneous Point Source in the Atmospheric Surface Layer', *Boundary-Layer Meteorol.* **71**, 341–373.

Yee, E., Chan, R., Kosteniuk, P. R., Chandler, G. M., Biltoft, C. A., and Bowers, J. F.: 1995, 'The Vertical Structure of Concentration Fluctuation Statistics in Plumes Dispersing in the Atmospheric Surface Layer', *Boundary-Layer Meteorol.* **76**, 41–67.

Zimmerman, W. B. and Chatwin, P. C.: 1995, 'Fluctuations in Dense Gas Concentrations Measured in a Wind-Tunnel', *Boundary-Layer Meterol.* **75**, 321–352.